Reviewed Preprint
v1 • November 19, 2025
Not revised

Reviewed Preprint
v2 • June 17, 2026
Revised by authors

Bidirectional redistribution of actomyosin drives epithelial invagination in ascidian siphon tube morphogenesis

Jinghan Qiao[1,#], Pengyu Yu[2,#], Hongzhe Peng[1], Wenjie Shi[1], Bo Li[2] ✉, Bo Dong[1,3] ✉

[1]Fang Zongxi Center, MoE Key Laboratory of Marine Genetics and Breeding, College of Marine Life Sciences, Ocean University of China, Qingdao, China • [2]Institute of Biomechanics and Medical Engineering, Applied Mechanics Laboratory, Department of Engineering Mechanics, Tsinghua University, Beijing, China • [3]Institute of Evolution & Marine Biodiversity, Ocean University of China, Qingdao, China

For correspondence:
libome@tsinghua.edu.cn
bodong@ouc.edu.cn

[#] These authors contribute equally to this work

Competing interests: No competing interests declared

Funding: See page 25

Reviewing editor: Deborah Yelon, University of California, San Diego, United States

eLife Assessment

This **useful** study uses a combination of experimental and modeling approaches to investigate the role of actomyosin in epithelial invagination during Ciona siphon tube morphogenesis. Several types of **solid** quantitative analyses and modeling approaches are presented that support a model in which bidirectional relocation of actomyosin drives invagination. Since epithelial invagination contributes to the morphogenesis of many developing organs, this work has the potential to appeal to both cell biologists and developmental biologists.

https://doi.org/10.7554/eLife.108588.2.sa4

Abstract

How epithelia perform a spatiotemporal heterogeneous force generating program to drive a sequential tissue morphogenesis remains unclear, particularly the underlying precise mechanical mechanisms. This study investigated dynamic actomyosin reorganization between apical and lateral membrane cortex regions during two sequentially invaginated stages during ascidian atrial siphon tube morphogenesis. At the initial invagination stage, the originally lateral-located actomyosin redistributed to the apical domains, while those actomyosin redistributed back to lateral domains at the accelerated invagination stage. Using genetic mutants to modulate myosin activities, the initial invagination was strengthened or abolished, indicating invagination is apical constriction dependent. Optogenetic inhibition of myosin activities in lateral domains after initial invagination stage blocked the further processes, suggesting lateral constriction of actomyosin is required for the accelerated invagination. Vertex model simulations uncovered a coupled mechanism underlying epithelial invagination driven by apicobasal tension imbalance and lateral contraction. We thus propose an actomyosin redistribution mechanical model: lateral actomyosin first redistributes apically to drive apical constriction and shape the initial invagination, then apical actomyosin redistributes laterally to promote lateral contractility and accelerate invagination. Our findings reveal a bidirectional reorganization of actomyosin network as a central mechanism driving epithelial invagination, providing insights on epithelial invagination and the organ morphogenesis during development.

Introduction

Morphogenesis, by which cells and tissues acquire their shape and structure, is a central theme in developmental biology. The tissue shape transformation in morphogenesis is fundamentally driven by the spatiotemporally regulated biomechanical forces (Collinet & Lecuit, 2021; Matter &

Balda, 2003; Štorgel et al., 2016). The generation and conduction of biomechanical forces play as an essential mechanism of morphogenesis, via regulating cell rearrangement, division, and deformation at both cellular and tissue scales (Chan et al., 2017; Lecuit et al., 2011; Matter & Balda, 2003; Nagafuchi, 2001; Osswald et al., 2022; Tepass, 2002). Among these, actomyosin contractility plays a pivotal structure generating biomechanical tension in subcellular level, which is the basic of cell and tissue-level morphogenesis (Chung et al., 2017; Even-Ram et al., 2007; Fristrom, 1988; Lee & Harland, 2007; Popkova et al., 2024; Vicente-Manzanares et al., 2009; Zartman & Shvartsman, 2010). Despite the widely acknowledged critical role of bio-mechanical forces in morphogenesis, the precise mechanisms by which these forces regulate cell and tissue remodeling, particularly how cells reorganize contractile domains in space and time to coordinate sequential morphogenetic events remains a significant challenge.

A typical example of morphogenesis is the transition from simple epithelial sheets to complex three-dimensional architectures (Collinet & Lecuit, 2021). A large number of previous researches demonstrated the function of apical constriction in epithelial sheet invagination, such as in the invagination process of the *Drosophila* embryonic trachea (Schottenfeld et al., 2010) and salivary gland placode (Pearl et al., 2017). However, more and more studies noticed that the apical constriction itself is not sufficient in shaping complex epithelial three-dimensional structures and various epithelial tube shapes (Kondo & Hayashi, 2013; Pearl et al., 2017). So, an interesting question is how do epithelial cells preform a spatiotemporal heterogeneous force generating program to drive a sequential epithelial tissue reshaping.

Marine ascidian *Ciona* is an excellent model for studying morphogenesis due to its simple developmental process, transparent embryos, and its close evolutionary relationship with vertebrates (Blair & Hedges, 2005; Delsuc et al., 2006; Zhao et al., 2021). For example, asymmetrical actomyosin contractility in notochord was demonstrated to provide force for tail bending (Lu et al., 2020; Peng et al., 2020). Local myosin activation coupled with junctional rearrangements drives directional zippering (Fiuza & Lemaire, 2021; Hotta et al., 2007; Kourakis et al., 2010) in neural tube closure, cell cortex distribution, and the stability of tight junctions (TJs) were essential for notochord tube lumen opening and expansion (Shi et al., 2025). Actomyosin sequentially localized on the apical and basolateral cell surfaces to drive the endodermal invagination (Fiuza & Lemaire, 2021; Hotta et al., 2007; Kourakis et al., 2010). However, this transition is from apical to basolateral (Sherrard et al., 2010), rather than a bidirectional redistribution between apical and lateral domains. Similarly, in *Drosophila* gastrulation, apical constriction initiates ventral furrow formation, but lateral myosin is not absolutely required for the later stages; indeed, the second phase of invagination can proceed even when lateral contractility is compromised (Guo et al., 2022). Whether a bidirectional redistribution of actomyosin between apical and lateral domains operates as a core mechanism for sequential invagination, and whether lateral contractility is essential for the accelerated phase, remain unclear.

Ciona and vertebrates share evolutionary developmental homology. There may be a potential homology between the otic placode of vertebrates and the atrial siphon primordium of *Ciona* (Kourakis et al., 2010). The atrial siphon forms from a non-dividing region in the lateral-dorsal epidermis of the head and follows a separate developmental trajectory (Hotta et al., 2020; Kourakis et al., 2010). Invagination initially generates shallow pits, which later deepen and connect to the gut lumen after metamorphosis, creating two atrial siphons (Hotta et al., 2007; Kourakis et al., 2010). Eventually, the left and right siphons fuse to form a single atrial siphon (Chiba et al., 2004). Despite these observations, the early cellular events during atrial siphon tube morphogenesis remain incompletely understood.

In this study, we investigated the morphogenesis of the *Ciona* atrial siphon. Firstly, the detailed cellular process of *Ciona* atrial siphon formation through initial and the accelerated stages was described by visualizing cell boundary and nuclei. By combining actomyosin localization analysis, genetic manipulation, and vertex model simulations, we demonstrated that lateral actomyosin first redistributed apically to drive apical constriction and established the initial invagination, then redistributed laterally to promote cell shortening and the further atrial siphon tube

invagination. Disruption of myosin activity altered invagination timing, while optogenetic inhibition of myosin activity after initial apical constriction stage blocked the further invagination. Furthermore, a cell-based vertex model was established to validate the relationship between contractile force redistribution and epithelial invagination. The coupled biomechanical mechanisms induced by apicobasal imbalance and lateral contraction were uncovered as fundamental determinants of the atrial siphon invagination. These results provide new insights into the biomechanical control of tissue morphogenesis, and highlight the value of marine model organisms for addressing fundamental questions in developmental biology.

Results

The cellular processes of *Ciona* atrial siphon invagination

To investigate the early cellular events during atrial siphon morphogenesis, we performed actin filament (F-actin) staining on the fixed samples to capture the detailed cellular dynamics (Figure 1A). The cell at the bottom center of the invaginating region was defined as the "center cell" (Figure 1B). Measurements taken at different stages included the height and apical-to-basal area ratio of the center cell, the invagination depth of the atrial siphon and the linear distance between the −3/−4 and +3/+4 cell junctions (Figure 1B-E, Figure 1—figure supplement 1). At the initial invagination stage (13.5-16.0 hpf), the center cell height increased, the apical-to-basal area ratio decreased, and the protruding cell surface became inward pit, but no significant invagination occurred (Figure 1A), as reflected by a low invagination slope (k = 0.2617). During the accelerated stage (16.0-18.0 hpf), the center cell height decreased, the apical-to-basal area ratio stabilized, and invagination progressed rapidly (k = 2.7920). EdU incorporation and TUNEL assays demonstrated that neither cell division nor apoptosis was involved in the whole invagination process (Figure 1—figure supplement 2).

Bidirectional redistribution of actomyosin between apical and lateral domains during atrial siphon tube invagination

To analyze the forces driving atrial siphon tube invagination, we first visualized the distribution of F-actin and quantified its dynamics at different cellular domains (Figure 1—figure supplement 1A). During the initial invagination stage, before 15 hpf, F-actin concentration decreased at the lateral domains, while gradually increasing around the apical membrane, resulting in a higher F-actin accumulation at the apical region. Subsequently, the F-actin concentration at lateral region started to increase and exceeded that in the apical domain at 16 hpf (Figure 1—figure supplement 1A).

Using anti-pS19 MRLC antibody, we examined the spatial and temporal patterns of myosin activity within the atrial siphon primordium. Quantification of signal intensities from the apical, basal, and lateral regions during the initial and the accelerated stages showed that active myosin underwent a clear bidirectional redistribution (Figure 2A, B). During the initial invagination stage (before 16 hpf), myosin activity shifted from the lateral to the apical domain, resulting in higher apical levels. In contrast, during the accelerated stage (after 16 hpf), myosin redistributed from the apical to the lateral domain, leading to predominant lateral enrichment (Figure 2B). This redistribution pattern was consistent with that of F-actin in the corresponding phases.

Additionally, top view imaging showed that during the initial stage, atrial siphon primordium cells were arranged in a circular pattern (Figure 2A). Active myosin exhibited a similar ring-like localization, and this ring-like pattern extended to about 15–20 cells of the primordium, indicating that the early stages of atrial siphon morphogenesis are driven by circumferential contractile forces generated by phosphorylated myosin, facilitating inward constriction of the primordium (Figure 2A, B). Furthermore, quantification of the lateral cell distance (Figure 1—figure supplement 1B) demonstrated a reduction in spacing between peripheral cells, indicating that surrounding cells moved centripetally toward the center position.

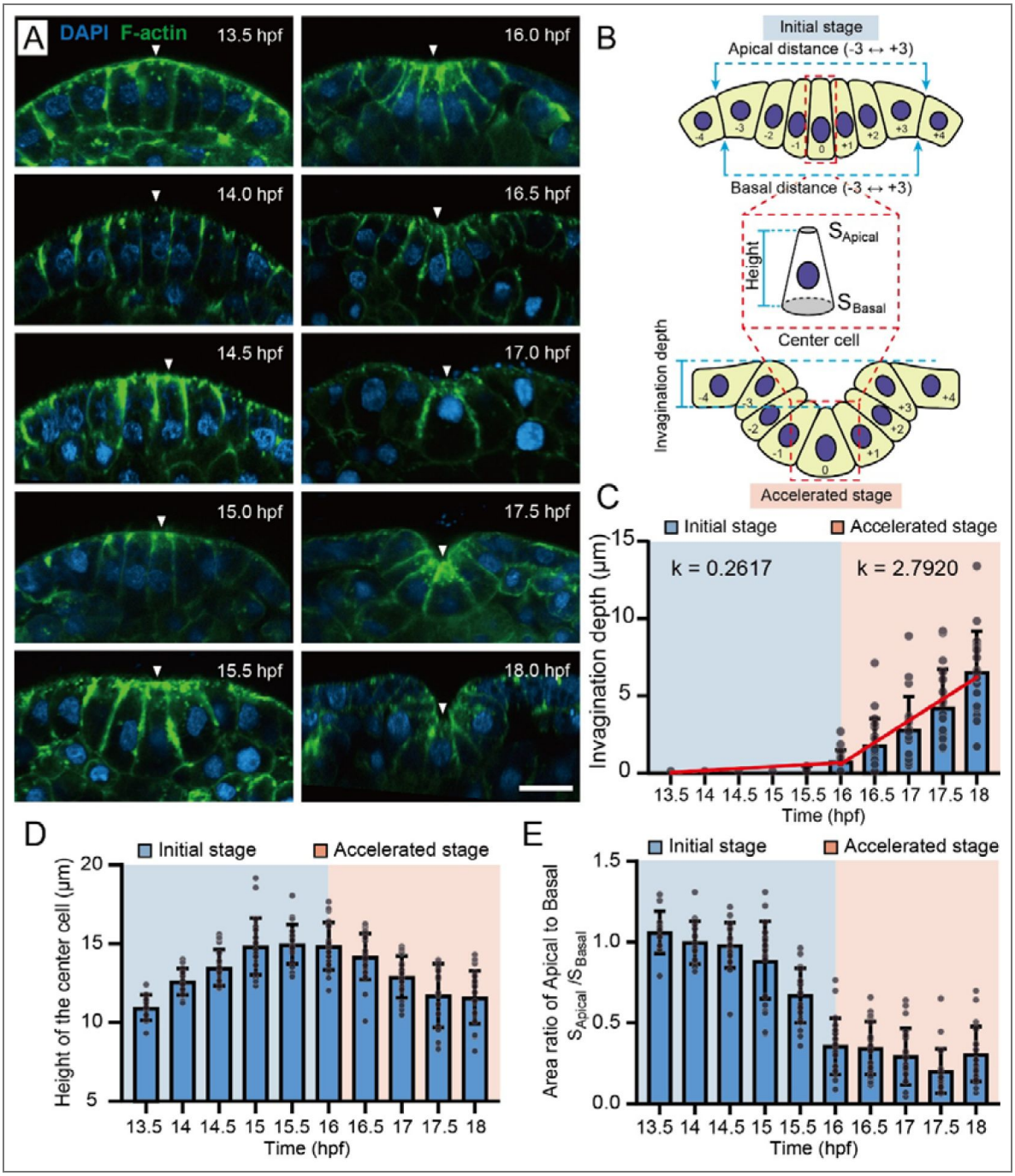

Figure 1. Cellular processes of *Ciona* atrial siphon tube invagination.

(A) Representative images of atrial siphon morphogenesis in *Ciona* embryos from 13.5 hpf to 18 hpf. The white arrow indicates the central cell. Scale bar: 10 μm. (B) Measurement parameters of the *Ciona* atrial siphon. The cell undergoing the most prominent apical constriction at the center of invagination was defined as the center cell (0). The adjacent cells on the left and right were defined sequentially as −1, −2, −3, −4 and +1, +2, +3, +4, respectively. (C) Quantification of the invagination depth in the atrial siphon of *Ciona* embryos. Red lines indicate linear regression fits of invagination depth during the initial (13.5-16 hpf, k = 0.2617) and accelerated (16-18 hpf, k = 2.7920) stages. n = 20. (D, E) Quantification of the center cell height and apical-to-basal area ratio at the atrial siphon of *Ciona* embryos. The blue-shaded region represents the initial stage, while the orange-shaded region indicates the accelerated stage. N = 20.

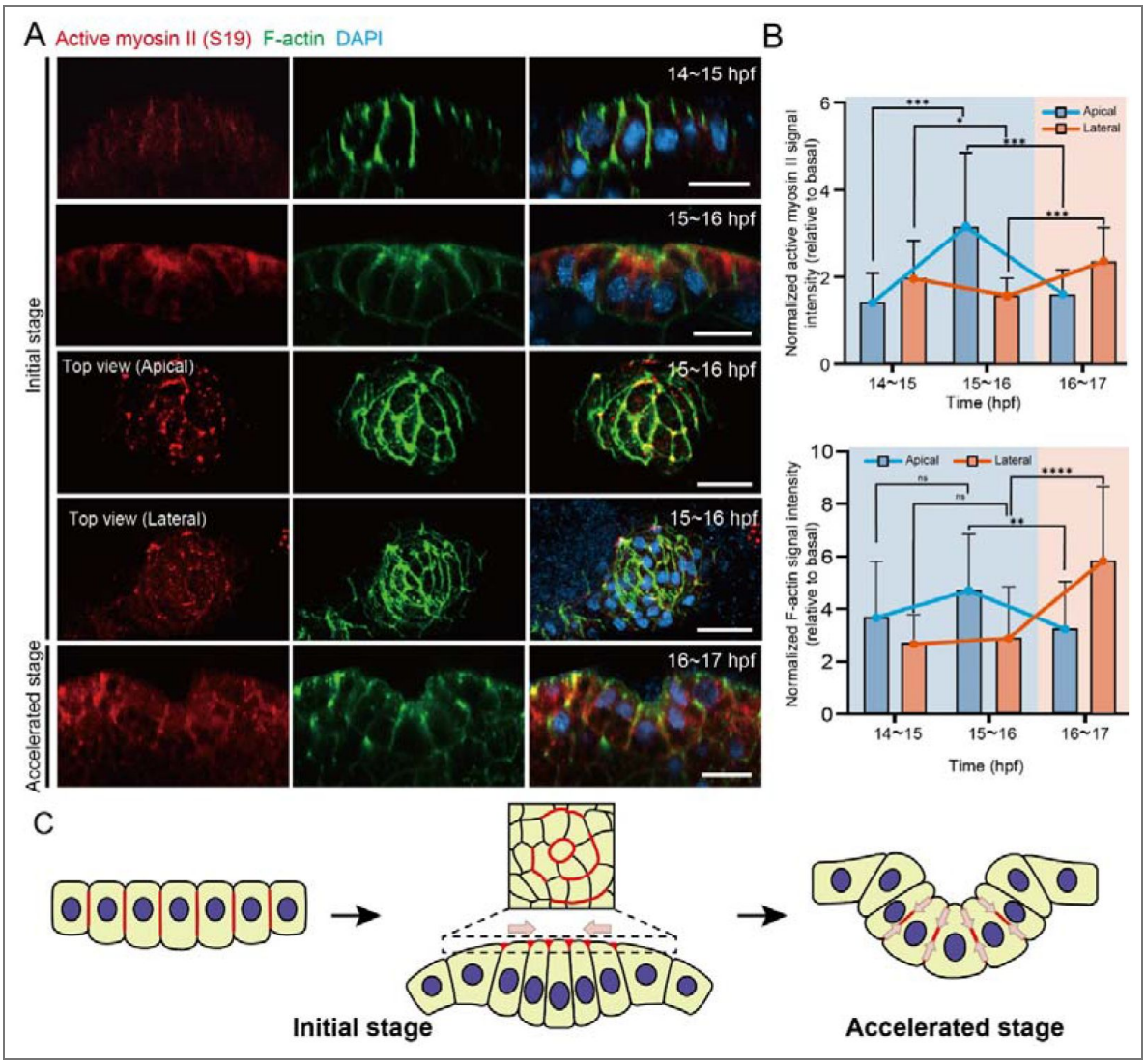

Figure 2. Bidirectional redistribution of actomyosin between apical and lateral domains during atrial siphon tube invagination.

(A) Representative images of *Ciona* embryos stained for active myosin II (anti-pS19 MRLC, red) and F-actin (green) at different stages of atrial siphon invagination. Scale bar: 10 μm. (B) Normalized fluorescence intensity of active myosin II (anti-pS19 MRLC) and F-actin at the apical and lateral regions of center cells during different stages of atrial siphon invagination (basal level set to 1). The blue-shaded region represents the initial stage, while the orange-shaded region indicates the accelerated stage. $^{**}p < 0.01$, $^{***}p < 0.001$, $^{****}p < 0.0001$, n = 20. (C) Schematic model illustrating the mechanical forces driving atrial siphon primordium invagination. Brown arrows indicate the direction of contractile forces; red areas depict active myosin II localization.

Integrating the localization of actomyosin with the observed cell shape changes, we propose a hypothesis in which the bidirectional reorganization of contractile forces at the apical and lateral regions drives epithelial invagination during atrial siphon morphogenesis (Figure 2C). Initially, actomyosin redistributed from the lateral regions to the apical domains, generating contractile forces for apical constriction (Figure 1—figure supplement 1A). Meanwhile, the inward compression from surrounding cells facilitates cell elongation, establishing the initial invaginated cell morphology and preparing for subsequent morphogenesis (Figure 1—figure supplement 1B). Then, actomyosin redistributed from the apical domains to the lateral regions, generating contractile forces that promoted center cell shortening and accelerated the tissue invagination (Figure 2C).

Center cell height is coupled with invagination depth

To further verify our hypothesis and explore the relationship between myosin contractility, force redistribution, and the progression of invagination, we overexpressed MRLC (T18ES19E)::mCherry (a diphosphorylated mutant that enhances myosin activity) (Espinoza-Fonseca et al., 2014), MRLC (T18AS19A)::mCherry (an unphosphorylated mutant that reduces myosin activity) (Iwasaki et al., 2001) and MRLC::mCherry (wild-type control) in the atrial siphon primordium to modulate contractile force in embryos, respectively (Figure 3A, B). The results showed that the invagination initiated earlier (15 hpf) compared to control group in MRLC (T18ES19E)-expressed embryos. At 16 hpf, MRLC (T18ES19E) group exhibited a deeper invagination and shorter center cell height. In contrast, in MRLC (T18AS19A) group, the invagination initiation time was delayed. Even at 16 hpf, the center cell height did not decrease and the invagination did not occur (Figure 3B). Notably, the increase in invagination depth is strongly correlated with the reduction in center cell height, with both changes occurring synchronously across experimental groups with different myosin activities (Figure 3B). These results demonstrate a strong coupling between the reduction in center cell height and the increase in invagination depth, suggesting that this process is closely associated with the redistribution of myosin localization from the apical to lateral regions as invagination progresses.

Inhibition of myosin activity during apical-to-lateral redistribution impedes invagination progression

To further examine the necessity of the redistribution of myosin between the apical and lateral regions during invagination, we utilized an optogenetic MLCP-BcLOV4 (Berlew et al., 2021; Berlew et al., 2020; Berlew et al., 2022; Glantz et al., 2019; Glantz et al., 2018; Yamamoto et al., 2021) system (Figure 4A) to specifically inhibit myosin II activity at the critical redistribution time point between the initial invagination and the accelerated invagination stage (16-17 hpf). This system has been proven to effectively reduce the contractility of epidermal cells in *Ciona* embryos (Qiao et al., 2023). Compared to the control group (Figure 4—figure supplement 1) and dark treatment group, the experimental group with 1 h light exposure, which activated the optogenetic system, blocked further invagination (Figure 4B, Figure 4—video 1, 2), and while invagination ceased to deepen, the center cell height did not show a significant decrease (Figure 4C, D). Immunostaining of active myosin (p-MLC) revealed that after light exposure, lateral myosin intensity was significantly reduced compared to the dark control group, whereas apical myosin levels decreased similarly in both groups (Figure 4— figure supplement 2). This indicates that the optogenetic manipulation effectively attenuates lateral contractility during the accelerated invagination stage without affecting the concurrent changes in apical contractility. Together, these results confirm that the redistribution of myosin contractility from the apical to lateral regions, specifically the acquisition of lateral contractility, is essential for the progression of invagination.

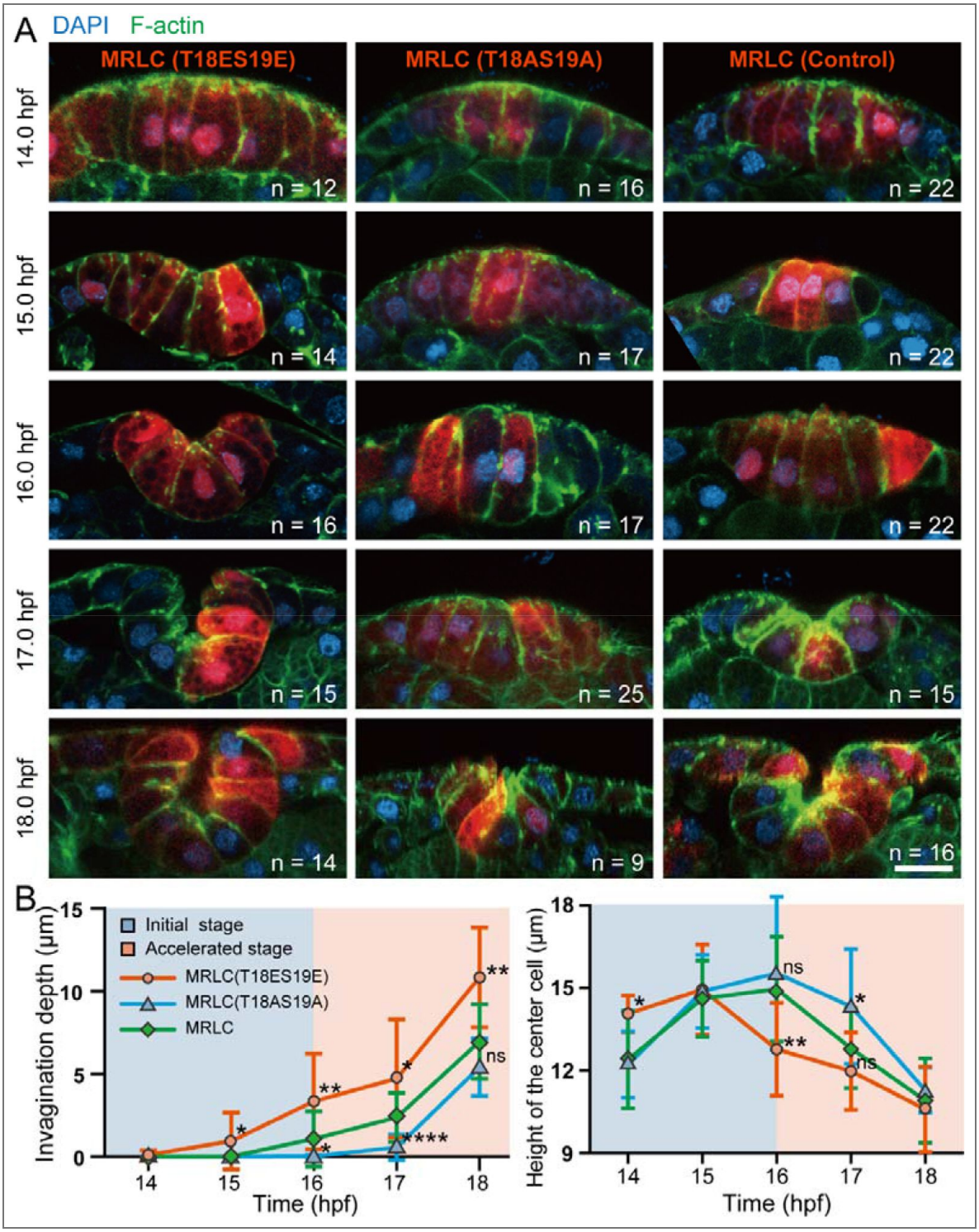

Figure 3. Modulation of atrial siphon invagination by overexpression of myosin mutants

(A) Representative images of *Ciona* atrial siphon primordium expressing wild-type and mutant MRLC constructs. Scale bar: 10 μm. (B) Quantification of invagination depth and the center cell height in MRLC (T18ES19E), MRLC (T18AS19A), and MRLC groups. The blue-shaded region represents the initial stage, while the orange-shaded region indicates the accelerated stage. *$p < 0.05$, **$p < 0.01$, ***$p < 0.001$, ****$p < 0.0001$.

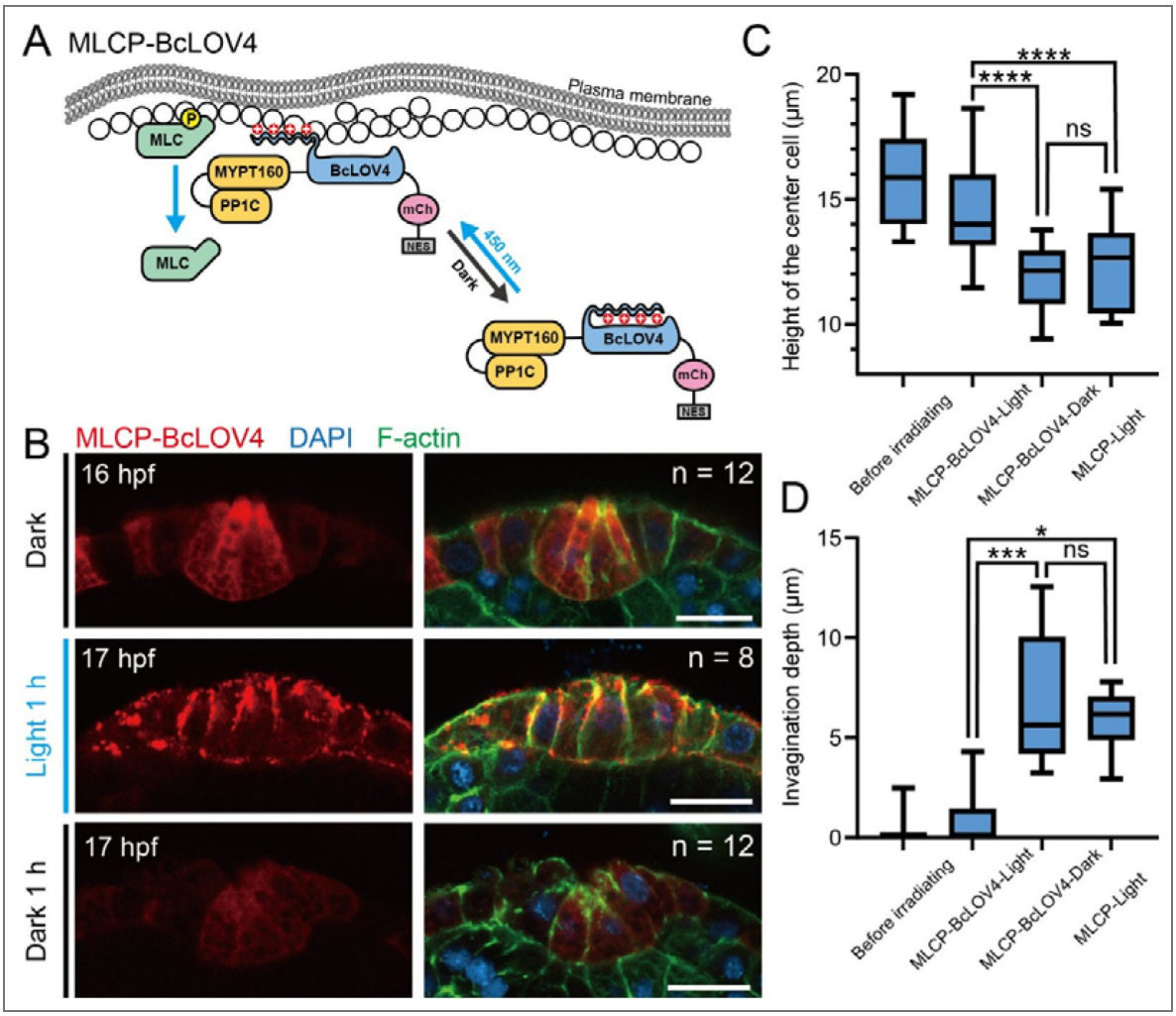

Figure 4. Disruption of contractile forces during rapid invagination of the *Ciona* atrial siphon using an optogenetic system

(A) Schematic diagram depicting the structure and mechanism of the MLCP-BcLOV4 system. The PP1C::MYPT169::BcLOV4::mCherry::NES fusion protein is initially dispersed in the cytoplasm. Upon exposure to blue light, BcLOV4 undergoes a conformational change, allowing it to interact electrostatically with the plasma membrane. This leads to the recruitment of the PP1C and MYPT169 components, subunits of myosin light chain phosphatase (MLCP), to the membrane, where they reduce myosin activity. (B) Representative images of developmental progression in the MLCP-BcLOV4 expression group exposed to blue light for 1 h, and in the dark control group maintained in darkness for 1 h. Scale bar: 10 μm. (C, D) Quantification of invagination depth and the center cell height in the MLCP-BcLOV4 expression group, the dark control group and MLCP control group (Figure 4—figure supplement 1). *$p < 0.05$, ***$p < 0.001$, ****$p < 0.0001$.

Vertex model simulations recapitulate the mechanical process of ascidian siphon tube invagination

The morphological invagination of epithelial tissues is a conserved mechanical process across diverse developmental contexts. In the early ascidian embryo, a small-scale endoderm plate of only ten cells undergoes invagination via a two-step program of apical constriction and basolateral cell shortening (Sherrard et al., 2010). While the redistribution of actomyosin in this system closely mirrors what we observe in the siphon primordium, their gastrulation-stage movement represents a global evolution of embryonic geometry. In contrast, the invagination of the atrial siphon is a distinctly localized active process within a much larger tissue. A more analogous and extensively studied system is the *Drosophila* ventral furrow formation (VFF), where apical constriction initiates the initial tissue bending (Brodland et al., 2010; Polyakov et al., 2014). The progression into a deep fold further requires lateral contractility (Conte et al., 2012), and is significantly facilitated by in-plane compressive stresses generated by the surrounding tissues (Guo et al., 2022). These studies have established and refined a vertex model framework, effectively elucidating the mechanical underpinnings of such morphogenetic events.

Notably, these classic vertex models of VFF typically incorporate the vitelline membrane—a rigid, non-adhesive extraembryonic shell that tightly encloses the embryo—as a boundary condition (Brodland et al., 2010; Conte et al., 2012; Guo et al., 2022; Polyakov et al., 2014). This membrane acts as a critical external constraint that prevents any outward expansion of the cells. Under such confinement, the mechanical strain generated by active contractility has no degree of freedom for outward displacement and can only be released through inward invagination into the yolk. However, in the case of the ascidian siphon, the larval head is enclosed only by a soft, elastic tunic, offering no such rigid mechanical constraint. In this relatively free-moving tissue, the mechanical mechanism by which a spatiotemporally regulated actomyosin redistribution drives invagination remains to be elucidated.

To evaluate how the bidirectional redistribution of actomyosin drives invagination, we developed a cell-based two-dimensional (2D) vertex model based on previous studies (Guo et al., 2022; Polyakov et al., 2014), and performed simulations for atrial siphon morphogenesis. The 2D cross-section of the *Ciona* embryo head along the transverse plane of its anterior-posterior axis was represented by polygonal cells connected in a circular arrangement, surrounding the inner cells (Figure 5A, Figure 5—figure supplement 1). Since the actomyosin redistribution is highly localized within the surface epithelium, we defined this domain as a local active region occupying an initial θ-degree arc of the entire circular tissue. To maintain structural integrity while focusing on epithelial mechanics, the internal cells were simplified as volume-incompressible bulk, providing mechanical support during the invagination process. Cell deformation and tissue morphology were simulated through vertex dynamics, governed by an effective energy functional that accounts for cell area conservation, passive cortical contractility, epithelial bending stiffness, and particularly spatiotemporally regulated active line tensions (Figure 5A, see Methods for details). The redistribution of actomyosin from apical to lateral domains was described by the temporal evolution of normalized intensities m_J^{a} and m_J^{l} on the apical and lateral edges of cell J. Following the normalization of F-actin intensity to the basal surface in experimental measurements (Figure 1—Figure supplement 1A), the model adopted the basal actomyosin intensity $\left(m_J^{\mathrm{b}} = m_0\right)$ as a non-contractile baseline. The active line tension on the apical or lateral domains was then formulated as $k_{\mathrm{m}}^{\mathrm{a,l}}\left(m_J^{\mathrm{a,l}} - m_0\right)$, representing the force generated by actomyosin enrichment above the basal baseline, with k_m serving as the tension coefficient. The intensity m within the active region was prescribed by a Gaussian distribution that is centered at the center cell (with index 0) and spans the seven active cells (from index −3 to +3) (Figure 5A, see Methods for details). At 13 hpf, the epithelial cross-section of the larval head comprises approximately 50 cells. Numerical simulations were therefore initiated using a circular epithelium of N= 50 cells to examine the morphological processes driven by active tensions (see Methods). Although the tissue expands and its geometry becomes flatter as development proceeds as observed experimentally (Figure 5—figure supplement 1), the size of the active region is much smaller than the total

tissue size. Thus, the model focused on the localized impact of actomyosin-driven deformation while omitting global tissue growth. The mechanical implications of tissue size evolution will be discussed further below.

Our mechanical model successfully reproduced the cell shape evolution and invagination of the atrial siphon observed in experiments (Figure 5C, D). During the initial stage, the rapid accumulation of actomyosin on the apical surface in the active region gives rise to apical tension. This localized contraction induces apical narrowing and leads adjacent cells to incline toward the center. The resulting cell elongation breaks the initial apicobasal symmetry, thereby initializing the invagination into the basal side during 15-16 hpf. After 16 hpf, the lateral actomyosin intensity increases significantly and induces high contractility on the lateral surface, pulling cells and shortening the cell height. The synergy between apical and lateral contraction further drives the invagination process, ultimately establishing the characteristic siphon-like epithelial architecture (Figure 5D). The invagination depth is quantified as the vertical distance from the apical surface of the center cell to a baseline connecting the apical junctions of cells ±4 and ±5, and the height of the center cell is defined as the vertical distance between its apical and basal surfaces. Both quantifications obtained from the simulations are consistent with the experimentally measured data (Figure 5C), which confirms the validity of our model in capturing the mechanical process of ascidian siphon tube invagination.

Note that, we find that "puckering" shape occurs surrounding the invagination in simulations (Figure 5D). Previous vertex models of VFF simulating cells within a rigid unmovable boundary do not exhibit this effect, and the invaginating cells remain tightly adherent, collapsing into a solid structure rather than forming a hollow tube (Conte et al., 2012; Polyakov et al., 2014). However, in our system of siphon morphogenesis, a tubular structure ultimately forms in the epithelium without strong boundary constraints. The final tubular structure is accompanied by significant F-actin accumulation at the apical surface (Figure 1A), which provides mechanical support and bending resistance (Hirashima & Matsuda, 2024; Wyatt et al., 2020). Thus, this "puckering" in our simulations arises from the bending energy, which enforces smooth curvature transitions along the circular surface. Actually, similar mild puckering is also observed *in vivo* at early stages (~ 17 hpf in Figure 1A), when the tissue size is small, but it rapidly disappears as the tissue grows and the geometry becomes flatter. Therefore, in our model, this shape discrepancy is expected to dimmish as the mean curvature decreases in a larger system (see Figure 6D). In addition, considering the cell-cell adhesion between the surface epithelium and internal bulk cells likely further suppresses this puckering in vivo, as outward evagination would require the coordinated deformation of underlying tissues.

Furthermore, we varied the apico-lateral actomyosin intensities $m = \alpha m_{\mathrm{exp}}$ by introducing a scaling factor α to the experimental measured value m_{exp} into the model, to simulate the unphosphorylated or diphosphorylated mutants with altered myosin activity (Figure 3). As expected, enhancement of both apical and lateral actomyosin activities increased the invagination depth while reducing the height of the center cell, and vice versa. These trends are consistent with the experimental mutant data (Figure 5A, B). That being said, the simulated invagination depth remains smaller than that observed experimentally across all conditions, and the invagination speed (represented by slopes of curves in Figure 5A) gradually slows down at later stages, in contrast to experiments. We attribute this discrepancy to the absence of growth-induced compressive stress in the model: as the invagination initiates, the furrow may act as a release site for accumulated internal stress, thereby accelerating its progression. This hypothesis requires validation through quantitative characterization of tissue size and stress distribution in the future. In addition, the final cell height in simulations is slightly larger than measured experimentally, because the model does not account for the mechanical constraints imposed by the growth of internal supporting tissues. Despite these differences, the results demonstrate that actomyosin contractility controls the magnitude of active forces and thereby regulates the morphology of invagination.

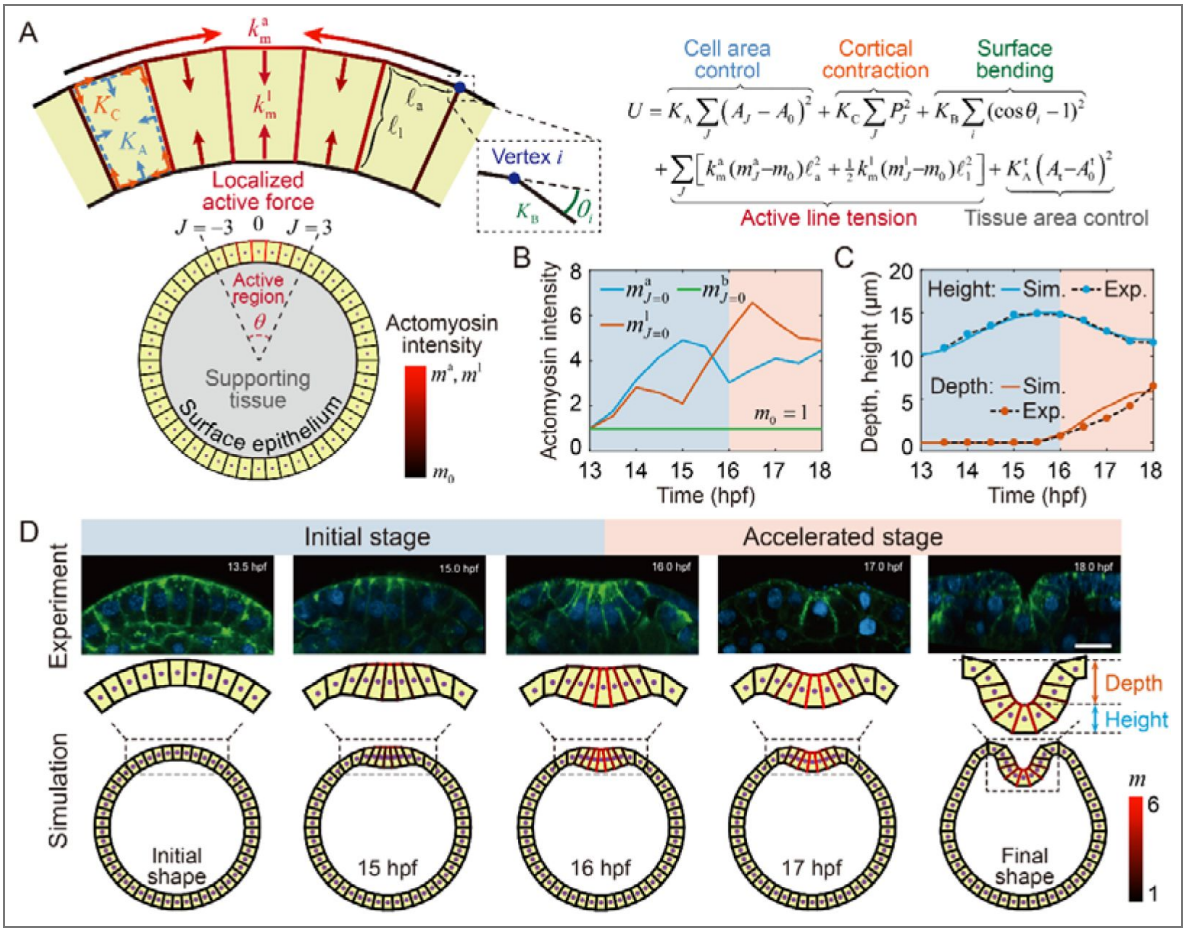

Figure 5. Vertex model simulations of siphon invagination.

(A) Schematic of cell-based vertex model. The epithelial tissue is represented by polygonal cells connected in a circular arrangement, surrounding inner supporting cells. The tissue is partitioned into an active region (consisting of cells with indices −3 to +3) with localized active forces, and an inactive region without actomyosin intensity. The effective energy U takes into cell area constraint (modulus K_A), passive cortical contraction (coefficient K_C), tissue surface bending (stiffness K_B), tissue area constraint (modulus K_A^t), and active line tensions on apical and lateral edges (coefficient k_m). (B) Temporal evolution of actomyosin intensities at apical, lateral, and basal domains of the center cell in the model, parameterized based on experimentally measured F-actin distribution. (C) Evolution curves of invagination depth (orange) and center cell height (blue) in simulations. Dots represent corresponding experimentally measured values. (D) Snapshots at specific timepoints during simulation progression (bottom), compared with corresponding experimental images (up). Colors on cell edges represent the normalized actomyosin intensity.

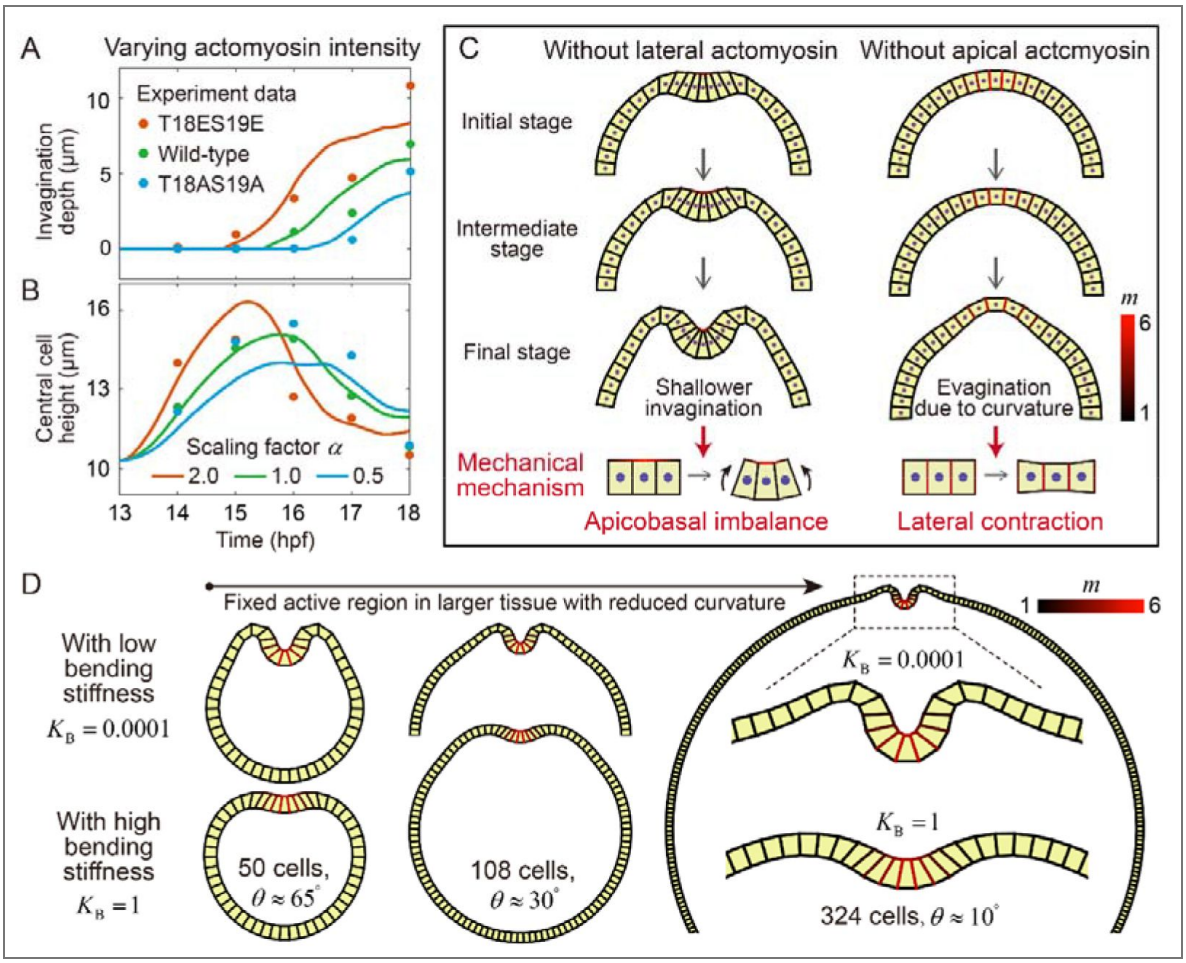

Figure 6. Mechanics of siphon invagination revealed by vertex model simulations.

(A, B) Invagination depth (A) and center cell height (B) regulated by changes in actomyosin intensities under the scaling factor *α* at both apical and lateral regions of all active cells. The data points are from the mutant experiments in Figure 3B. (C) Contributions of apical and lateral contractility. Simulations lacking lateral (left) or apical (right) activity result in shallower invagination or outward evagination, respectively, which highlight the distinct roles of apical constriction in initiating apicobasal imbalance and lateral contraction in driving deep folding. (D) Effects of tissue size and bending stiffness. With the active region size held constant, the global tissue curvature decreases as the total cell number increases. For *N*= 108, only the upper half of the tissue at K_B = 0.0001 is shown. For *N* = 324, a portion of the tissue is shown at K_B = 0.0001, and only the region near the active region is shown at K_B = 1.

Coupled mechanism of apicobasal tension imbalance and lateral contraction underlying epithelial invagination

To theoretically distinguish the effects of apical and lateral contraction on morphogenesis, we next performed simulations in which the two processes are considered independently. We considered active forces arising from either apical or lateral contraction alone, while maintaining the same actomyosin intensity profiles independently as in Figure 5B. We found that the apical contractility alone is sufficient to induce invagination, but produces a shallower invagination and taller cell shape in the absence of lateral actomyosin (Figure 6C). In contrast, without apical actomyosin, lateral contractility alone shortens the cells but cannot reproduce invagination. In a curved tissue with a surface bending modulus, such localized height reduction is more easily accommodated by bending outward. As a result, instead of driving invagination, lateral contraction biases the tissue toward outward deformation, leading to evagination (Figure 6C). These results suggest two successive mechanical mechanisms underlying the siphon invagination. An effective bending moment generated by apico-basal tension imbalance first breaks tissue symmetry and determines the location and direction of buckling. This is followed by a redistribution of actomyosin from the apical to the lateral domains, which drives lateral contraction to regulate cell shape and facilitate tissue invagination.

Finally, we investigate the proposal local active mechanisms under varying tissue curvature and bending stiffness. In the initial configuration (N= 50 cells), the active region spans approximately $\theta \approx 65^{\circ}$. However, in developing tissues, the length scale of the whole tissue is much larger than that of the active region. To examine this, we fixed the size of the active region

(seven cells) and constructed larger systems with N= 108 ($\theta \approx 30°$) and N= 324 ($\theta \approx 10°$), while keeping all other parameters unchanged. The resulting final tissue shapes are shown in Figure 6D. At low bending stiffness (K_B = 0.0001), pronounced local invagination emerges robustly across tissues with different curvature and system sizes, indicating that siphon invagination is governed by a highly localized active process that requires only apico-lateral contractions in a small group of cells. Notably, in the larger system with 324 cells, the puckering surrounding the invagination is significantly reduced because bending constraints are more prominent in highly curved tissues. As the tissue becomes flatter at later developmental stages, such puckering is therefore not expected to be observed experimentally. When the bending stiffness is increased (K_B = 1), local active contraction induces only cell shape changes and fails to drive invagination. This reflects a competition between local active contractile forces and the global mechanical resistance of tissue, suggesting that sufficiently strong active forces are required to overcome bending constraints and reshape tissue morphology. We note that the present model does not exclude the potential contribution of growth-induced compressive stresses, which may arise from tissue growth and augment the active mechanisms described above to accelerate invagination at later stages.

We plan to further elucidate this interplay in future work.

Discussion

The morphogenesis of the *Ciona* atrial siphon provides a compelling model to dissect how biomechanical forces orchestrate tissue invagination. Our study revealed that actomyosin contractility underwent a dynamic spatial redistribution during this process, initially redistributing from the lateral cortex to the apical region to promote apical constriction and establish the initial cell shape, and subsequently redistributing back to the lateral regions to promote center cell shortening and accelerate the tissue invagination. By combining actomyosin localization analysis, genetic perturbations, optogenetic manipulation, and vertex model, we established a mechanistic framework linking force dynamics to tissue remodeling. This work not only advances our understanding of siphon morphogenesis but also offers broader insights into the principles governing force-driven tissue shaping in developing organisms.

Sequential activation of actomyosin contractility has been documented in several epithelial folding systems, yet our study reveals distinct features. In ascidian endoderm invagination, actomyosin shifts from apical to basolateral regions (Sherrard et al., 2010), whereas our system exhibits bidirectional redistribution between apical and lateral domains, with the basal domain playing a passive role. More notably, during *Drosophila* ventral furrow invagination, lateral contractility is not essential for the second folding phase (Guo et al., 2022); in contrast, our optogenetic inhibition demonstrates that lateral contractility is obligatory for the accelerated stage. These comparisons establish bidirectional actomyosin redistribution as a distinct mechanical paradigm for sequential morphogenesis.

Our findings demonstrated that the atrial siphon invagination was driven by a coupled mechanism including apicobasal tension imbalance and lateral contraction in a two-stage process. During the initial stage (13.5-16.0 hpf), actomyosin redistributed from the lateral cortex to the apical cortex, generated contractile forces that induced apicobasal tension imbalance and reduced apical cell area and elongated the primordium. A transient actomyosin ring surrounding the primordium is prominent at the early initial stage and may cooperate with apical constriction, but it diminishes during the accelerated stage, indicating that sustained compression is not required. This aligns with classical models of epithelial folding, where apical actomyosin networks drive tissue curvature through localized contraction, often accompanied by an increase in cell height, as observed in the invagination of the *Drosophila* embryonic trachea (Schottenfeld et al., 2010) and salivary gland placode (Pearl et al., 2017). Future experiments using laser ablation or optogenetic inhibition specifically targeting this actomyosin ring could help dissect its precise contribution during the early invagination stage. Additionally, in traditional invagination models, various epithelial tissues use different mechanisms to drive deeper invagination. For example, in *Drosophila* tracheal development, mitosis acts as a critical turning point in accelerating invagination (Kondo & Hayashi, 2013). During the early slow phase of tracheal invagination, apical constriction under EGFR signaling forms a shallow pit. As invagination transitions into a rapid phase, mitotic entry induces cell rounding, which increases tension and epithelial buckling, thereby accelerating the invagination process and facilitating the internalization of placode cells (Kondo & Hayashi, 2013; Nishimura et al., 2007). Moreover, cell apoptosis can also expedite the invagination process, as seen in *Drosophila* leg morphogenesis, where actomyosin cables formed in apoptotic cells help trigger the invagination (Kiehart, 2015; Manjón et al., 2007; Monier et al., 2015). In *Drosophila* ventral furrow formation, in-plane compressive stresses generated by surrounding tissues significantly facilitate the deep fold (Guo et al., 2022). Distinct from these classical models, the accelerated invagination stage of *Ciona* atrial siphon morphogenesis was driven by a critical redistribution of apical actomyosin to the lateral regions, providing a force-generating mechanism for invagination progression without relying on cell proliferation or apoptosis to accelerate the process. The lateral enrichment of p-MLC correlated with a reduction in center cell height and the initiation of invagination, suggesting that lateral forces actively pulled the tissue inward. This spatial redistribution of contractile forces in *Ciona* atrial siphon invagination is reminiscent of mechanisms observed in certain epithelial folding processes, such as the *Drosophila* wing disc, where invagination is not solely driven by apical constriction but can also result from increased lateral tension or reduced basal tension (Sui et al., 2018). Our optogenetic inhibition of myosin activity during the apical-to-lateral redistribution—using the MLCP-BcLOV4 system—directly confirmed that this redistribution was not merely a passive consequence of invagination but was an active driver of the process.

Our study revealed a strong coupling between cellular shape changes and tissue remodeling during *Ciona* atrial siphon invagination, where the reduction in center cell height was closely associated with invagination depth. Tissue morphogenesis emerges from the integrated actions of multiple cellular behaviors, such as contraction, adhesion, and migration, that work in concert to remodel epithelial architecture (Chan et al., 2017). The transmission of local cell-generated forces across tissues is further shaped by mechanical cues and geometric constraints, enabling the transformation of cellular-scale changes into organ-scale morphogenesis (Collinet & Lecuit, 2021). By perturbing myosin activity, we found that this coupling was directly regulated: dominant-negative myosin mutants delayed both processes, whereas hyperactive myosin

accelerated invagination. The quantitative agreement between vertex model analysis and experimental measurements validated the critical role of actomyosin contractility dynamics in linking cellular shape changes to tissue remodeling. Furthermore, the model also uncoupled the effects of the actomyosin in different domains, and predicted that stronger apical-lateral redistribution facilitates the rapid reduction in height of invaginating cell. The *Ciona* atrial siphon, which underwent invagination without cell proliferation or apoptosis, provided a minimal system for investigating the role of biomechanical forces in tissue remodeling. Our findings emphasized that the deformation of a few key cells under spatially precise mechanical regulation, along with their coordination with surrounding tissues, is crucial for proper morphogenesis.

While this study clarified the role of actomyosin redistribution in atrial siphon invagination, several open questions remain regarding the molecular mechanisms underlying this process. One key question is what molecular signals drive the apical-to-lateral redistribution of contractility. Possible candidates include Rho GTPase pathways (Martin et al., 2016), which regulate myosin activation; apical-basal polarity(Peng et al., 2020), which coordinate actin reorganization during morphogenesis; and mechanosensitive ion channels that respond to tissue strain (Jin et al., 2020). Additionally, the role of cell-cell adhesion and extracellular matrix remodeling in mediating force transmission during invagination requires further investigation. Using tension sensors or perturbing adhesion molecules may provide new insights into these interactions. In addition, our experimental system involves significant global tissue remodeling: as development proceeds, the number of cells increases and the tissue expands substantially, accompanied by classic growth-induced compressive stress (Guo et al., 2022). Although we did not directly measure such stress in the siphon primordium, we observed a progressive flattening of the overall tissue geometry, which likely facilitates invagination and lumen formation. While our experiments and vertex model confirm that active tension alone is sufficient to drive invagination, tissue growth and the associated mechanical constraints may play critical roles in achieving the final tubular architecture. Future studies should integrate tissue growth and mechanosensitive feedback into theoretical models, and experimentally quantify how growth-induced stresses cooperate with local actomyosin redistribution to robustly shape the atrial siphon. Although our vertex model effectively clarified the contribution of force redistribution to invagination, it does not account for tissue growth or the potential for mechanosensitive feedback on the generation and redistribution of actomyosin. Future theoretical developments should focus on integrating tissue growth and mechanochemical feedback linking molecular signaling with tissue-level deformation to explain robust morphogenesis.

Materials and Methods

Experimental animals' preparation and electroporation

Ciona adults were collected from the coast of Qingdao and Rongcheng, Shandong, China. They were maintained in the laboratory seawater circulation system under constant light conditions to maintain their stability. Mature eggs and sperm were separately collected from the dissected adults and subsequently mixed for fertilization. The Fertilized eggs were dechorionated in seawater containing 1 % sodium thioglycolate (T0632; Sigma), 0.05 % protease E (P5147; Sigma) and 0.032 M NaOH. The dechorionated eggs were then used for plasmid electroporation based on the previous technique procedure (Christiaen et al., 2009). Finally, the embryos were cultured in an agar-coated dish with microporous-filtered seawater in 18°C for further observation. Detailed key resource information is annotated in Appendix 1—table 1.

Plasmid construction

Ciona myosin II light chain (MRLC) was amplified with primers MRLC-F and MRLC-R (Table S1). MRLC-mCherry (Dong et al., 2011); MRLC(T18AS19A)-mCherry and MRLC(T18ES19E)-mCherry (Denker et al., 2015); MLCP-BcLOV4 and MLCP(Qiao et al., 2023) were amplified with the primers listed in Appendix 1—table 2. For embryos expressing MRLC constructs, only those in which the center cell and more than half of the surrounding cells in the primordium showed clear mCherry fluorescence were selected for quantification.

Immunofluorescence

Ciona embryos were fixed with stationary liquid (Sherrard et al., 2010), which consisted of 100 mM HEPES (pH 6.9); 100 mM EGTA (pH 7.0); 10 mM MgSO4; 2% formaldehyde; 0.1% glutaraldehyde; 300 mM dextrose and 0.2% Triton X-100 for 40 m at room temperature. Following fixation, the embryos were washed three times with PBS and subsequently incubated in PBST (PBS supplemented with 0.1% Triton X-100) for 30 m to enhance permeability. To reduce autofluorescence, embryos were treated with 0.1% sodium borohydride in PBS for 20 m at room temperature. For immunostaining, embryos were incubated with a 1:250 dilution of Phospho-Myosin Light Chain 2 (Ser19) antibody (#3671: Cell Signaling) at room temperature for 24 h. After three additional washes with PBS, a 1:200 dilution of Alexa Fluor 568 anti-Rabbit IgG (A11011: Invitrogen) was added and incubated at room temperature for 48 h. For cell boundary visualization, embryos were stained with Alexa Fluor 488 Phalloidin (A12379: Invitrogen) at a 1:200 dilution. Finally, after three washes with PBS, embryos were mounted in DAPI-containing mounting medium and prepared for imaging.

Imaging and optogenetics

Live imaging, photoactivation experiments, and image acquisition were performed using a Zeiss LSM 980 confocal microscope (Carl Zeiss). For optogenetic experiments, *Ciona* embryos were placed in a 35 mm glass-bottom dish for imaging. To activate the optogenetic system, the designated region of interest was exposed to a 488 nm laser for 1 h. The control group for dark treatment was placed in a dark box at the same temperature for 1 h.

Quantification and statistical analysis

All images were analyzed and quantified using ImageJ (version 1.54p, NIH) and Imaris (version 9.0.1, Bitplane). For intensity measurements of active myosin (p-MLC) and F-actin, the apical domain was defined as a segmented line (width 1 μm) drawn along the apical cell-cell junctions of the center cell; the lateral domain was defined as a line along the lateral membranes excluding the apical and basal regions; the basal domain was defined as a line along the basal surface. Fluorescence intensities were normalized to the basal intensity of the same center cell (set to 1). Statistical analyses were performed using GraphPad Prism 10.1.2. Data are presented as mean ± SEM. Comparisons between two groups were analyzed by two-tailed Student's t-test. Significance levels are indicated as $*p < 0.05$, $**p < 0.01$, $***p < 0.001$, $****p < 0.0001$; ns indicates not significant. Sample sizes (n) for each experiment are indicated in the corresponding figure legends.

Vertex model simulations

Model description

The 2D cross-section of the *Ciona* embryo head along the transverse plane of its anterior-posterior axis is represented by polygonal cells connected in a circle, surrounding the inner supporting tissue (Figure 5A). Each polygon is defined by a set of vertices and edges. Vertices on the apical surface of cells are subject to free boundary conditions, which differs from the previous models (Conte et al., 2012; Polyakov et al., 2014). We define the invagination domain as a local active region occupying an initial θ-degree arc of the entire circular tissue. To maintain structural integrity while focusing on epithelial mechanics, the internal cells are simplified as volume-incompressible bulk, providing mechanical support during the invagination process. Cell deformation and tissue morphology are simulated through vertex dynamics, governed by an effective energy functional

$$U = K_{\mathrm{A}} \sum_{J} \left(A_J - A_0\right)^2 + K_{\mathrm{C}} \sum_{J} P_J^2 + K_{\mathrm{B}} \sum_{i} \left(\cos\theta_i - 1\right)^2 \#$$

$$+ \sum_{J} \left[k_{\mathrm{m}}^{\mathrm{a}} \left(m_J^{\mathrm{a}} - m_0\right) \ell_{\mathrm{a}}^2 + \frac{k_{\mathrm{m}}^{\mathrm{l}}}{2} \left(m_J^{\mathrm{l}} - m_0\right) \ell_1^2 \right] + K_{\mathrm{A}}^{\mathrm{t}} \left(A_{\mathrm{t}} - A_0^{\mathrm{t}}\right)^2, \#(1)$$

where the five terms result from, respectively, cell area control, cell passive cortex contractility, tissue surface bending energy, active line tensions on apical and lateral surfaces,

as well as tissue area constraint. K_A is the cell area modulus, and A_J and A_0 are the current and preferred areas of the cell J, respectively. $K_{\mathrm{A}}^{\mathrm{t}}$ is the tissue area modulus, and A_t and A_0^{t} are the current and preferred areas of the supporting tissue. K_C denotes the passive cortical contraction coefficient of cells and P_J represents the cell perimeter. K_B denotes the bending stiffness of the cell monolayer, representing its resistance to curvature changes. Physically, this stiffness arises from the recruitment of F-actin and other cytoskeletal elements at the tissue surface, serving as a critical mechanical constraint that ensures structural stability under free boundary conditions. θ_i is the angle between the neighboring apical or basal edges of vertex i (Figure 5A). $k_{\mathrm{m}}^{\mathrm{a}}$ and $k_{\mathrm{m}}^{\mathrm{l}}$ are the tension coefficient of actomyosin (m^a and m^l) recruited the apical and lateral surfaces whose lengths are ℓ_{a} and ℓ_{l}, respectively.

Experimental measurements of F-actin intensity on apical and lateral surfaces were normalized to the basal surface (Figure 1—Figure Supplement 1A). Consequently, we set the basal actomyosin intensity to $m_J^{\mathrm{b}} = m_0$, serving as a non-contractile baseline. The active line tension on the apical or lateral domains is then formulated as $k_{\mathrm{m}}^{\mathrm{a,l}}\left(m_j^{\mathrm{a,l}} - m_0\right)$, representing the force generated by actomyosin enrichment above this basal baseline. Notably, since each lateral edge is shared by two neighboring cells, the coefficient $k_{\mathrm{m}}^{\mathrm{l}}$ is halved in the force calculation for each individual cell. $\sum_J$ stands for the summation over all cells and $\sum_i$ runs over all apical and basal vertices.

Based on experimental measurements, the F-actin signal intensity is highest in the central cell and rapidly attenuates in the neighboring cells. To capture this spatiotemporal evolution within the active region, the actomyosin intensity is prescribed by a Gaussian distribution centered at the center cell (J= 0). The intensity for any cell J is defined as

$$m_J = (m_{J=0} - m_0) \cdot e^{-\frac{|J|^2}{2\sigma^2}} + m_0, \tag{1}$$

where $m_{J=0}$ is the experimental value measured from the central cell (as shown in Figure 5B), and J denotes the cell index extending from the center. The parameter σ controls the width of the active zone. In accordance with experimental observations, we set σ= 1.8. This distribution effectively spans from J= −3 to +3, encompassing approximately seven active cells, while the actomyosin activity is set to m_0 for cells outside this region ($|J|$ > 3).

Simulation scheme

In the simulations, we set the cell number N= 50 and a free boundary condition. The central seven cells (index −3 to +3) are considered as active cells under contractile forces whose actomyosin intensity varies in different stages. The other cells are observed to be inactive whose actomyosin intensities are always equal to m_0. In our simulations, tissue morphogenesis is represented by vertices motion and cell deformation. The motion of vertex i obeys the Langevin equation

$$\eta \frac{\mathrm{d}\mathbf{r}_i}{\mathrm{d}t} = -\frac{\partial U}{\partial \mathbf{r}_i^{'}} \tag{2}$$

where η denotes the friction coefficient. The equation was numerically solved using the forward Euler method with a time step of 0.001, using MATLAB R2021a. Simulations are run until t = 500, which corresponds to 18 hpf in experimental development, given a characteristic time scale of τ = 36 seconds. The final tissue shape is obtained after the system has relaxed to a steady-state configuration. The length scale L = 8.91 μm is determined by the normalization of initial cell height h_0 in model under real center cell height. The other parameters are all normalized with the time scale τ, length scale L, and friction coefficient η. Dimensionless parameters are set as follows: KA =1, $K_{\mathrm{A}}^{\mathrm{t}} = 0.001$, K_{C} = 0.001, $\mathrm{K_B}$ = 0.0001, $k_{\mathrm{m}}^{\mathrm{a}} = 0.016$, $k_{\mathrm{m}}^{\mathrm{l}} = 0.002$, A_0 = 1, h_0 = 1.25, and $A_0^{\mathrm{t}} = \pi(R_0 - h_0)^2$, where $R0 = NA_0/(2\pi h_0)$ is the

radius of initial tissue configuration. These parameter values are determined by numerical simulations under which the simulated invagination depth and center cell height imitates the experimental observations.

Lead contact

Requests for further resources should be directed to, and will be fulfilled by, the lead contact, Bo Dong (*bodong@ouc.edu.cn*).

Materials availability

All unique/stable reagents generated in this study are available from the lead contact with a completed materials transfer agreement.

Data availability

Model code and data are available upon request, and any additional information required to reanalyze the data reported in this paper is available from the lead contact upon request.

Figure supplements

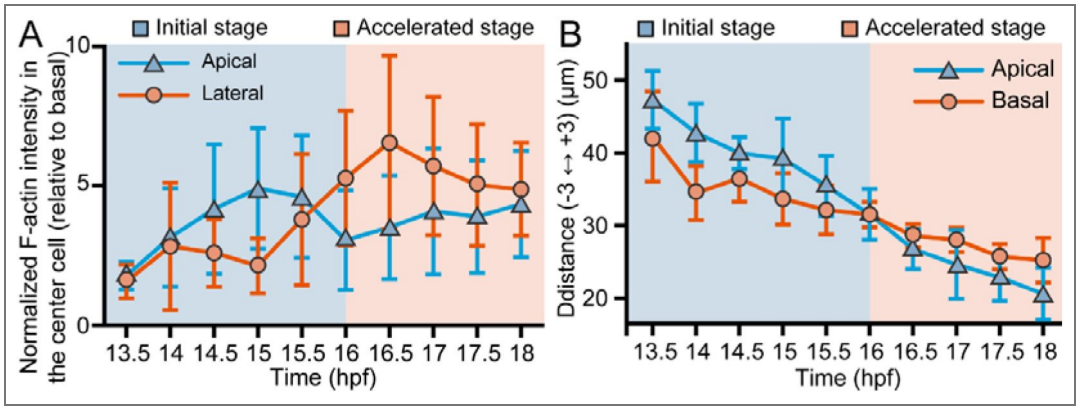

Figure 1—figure supplement 1. Quantification of F-actin intensity and intercellular distance during *Ciona* atrial siphon morphogenesis. (A) Normalized F-actin intensity at the apical and lateral regions of center cells during *Ciona* atrial siphon morphogenesis (basal level set to 1). (B) Quantification of the linear distance between the −3/−4 and +3/+4 cell junctions at the apical or basal surface in the atrial siphon of *Ciona* embryos. The blue-shaded region represents the initial stage, while the orange-shaded region indicates the accelerated stage. Representative images are shown in Figure 1A. n = 20.

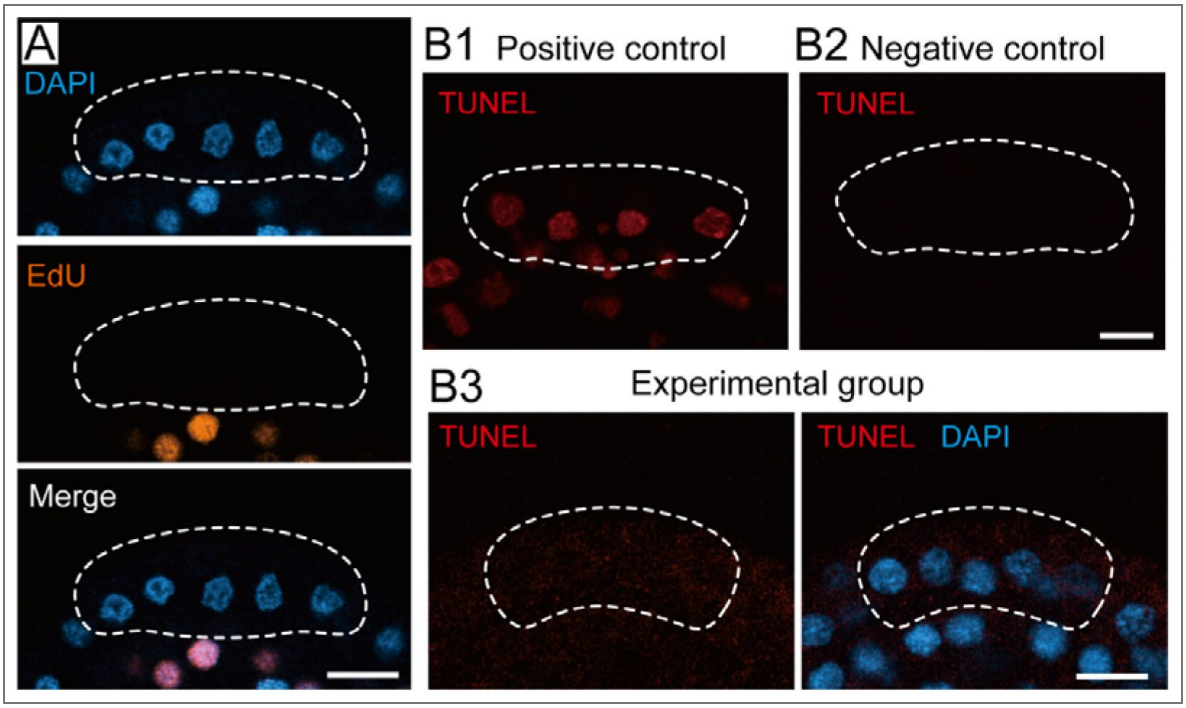

Figure 1—figure supplement 2. EdU and TUNEL staining during *Ciona* atrial siphon morphogenesis.

(A) Representative images of EdU staining at 14-15 hpf. Orange: EdU-positive nuclei indicating cell proliferation. Blue: DAPI. No EdU signal was detected in the atrial siphon primordium (white dashed outline). Scale bar: 10 μm. n = 10. (B) Representative images of TUNEL staining at 15 hpf. (B1) Positive control: DNase I pretreatment (20 U/mL, 10 min) induced DNA fragmentation. (B2) Negative control: staining performed without terminal deoxynucleotidyl transferase (TdT) enzyme. (B3) Experimental group: no detectable TUNEL signal in the atrial siphon primordium (white dashed outline). Scale bar: 10 μm. n = 10.

Figure 4—figure supplement 1. **MRCL control group in the optogenetic experiment**

(A) Schematic diagram depicting the structure and mechanism of the MLCP control system. The PP1C::MYPT169::mCherry::NES fusion protein remained diffuse in the cytoplasm under light exposure and failed to function. (B) Representative images of developmental progression in the MLCP control group exposed to blue light for 1h. Scale bar: 10 μm.

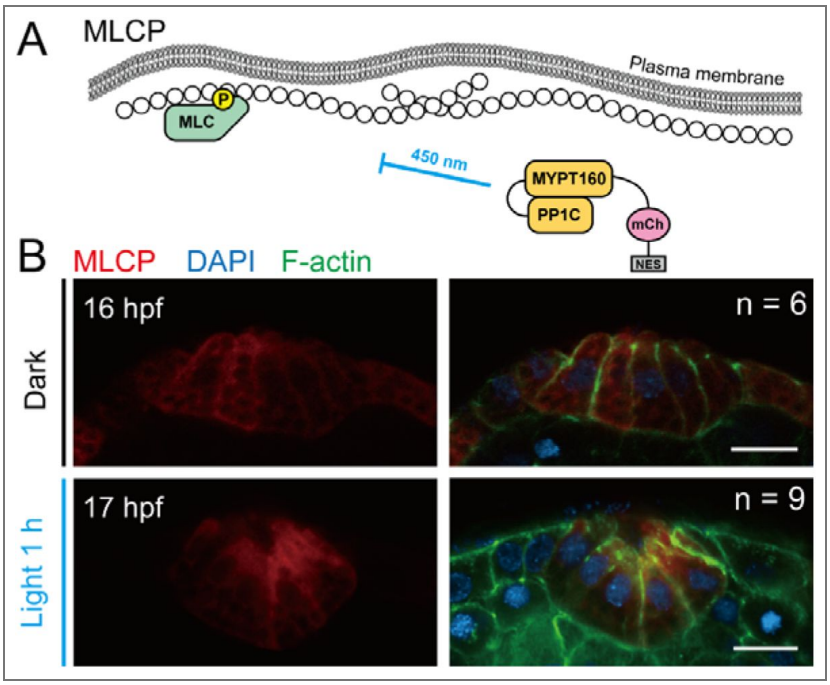

Figure 4—figure supplement 2. **Optogenetic inhibition effectively reduces the activity of lateral myosin.**

(A) Representative images of active myosin II (anti-pS19 MRLC, red) and F-actin (green) staining in the MLCP-BcLOV4-expressing embryos after 1 h of light exposure or dark control. Scale bar: 10 μm. (B) Quantification of normalized active myosin II intensity at the apical and lateral domains of the center cell. **p < 0.01.

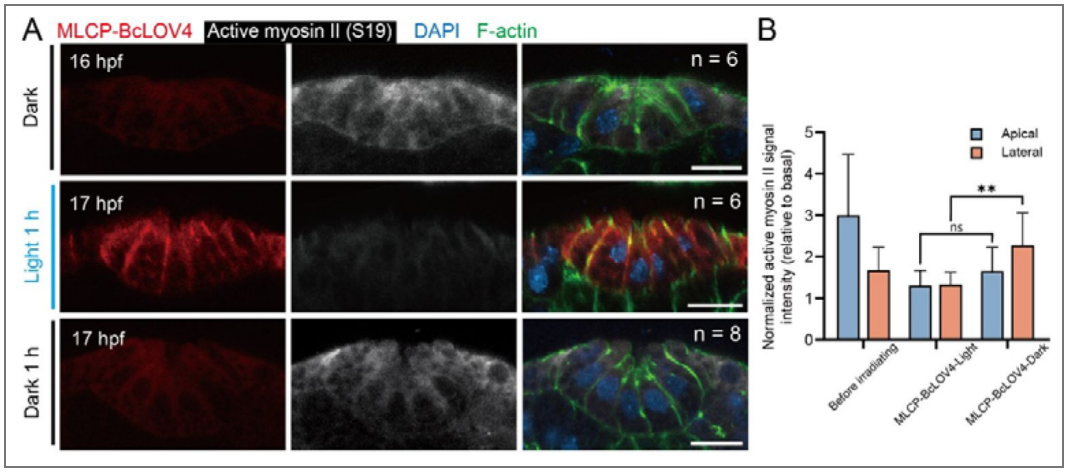

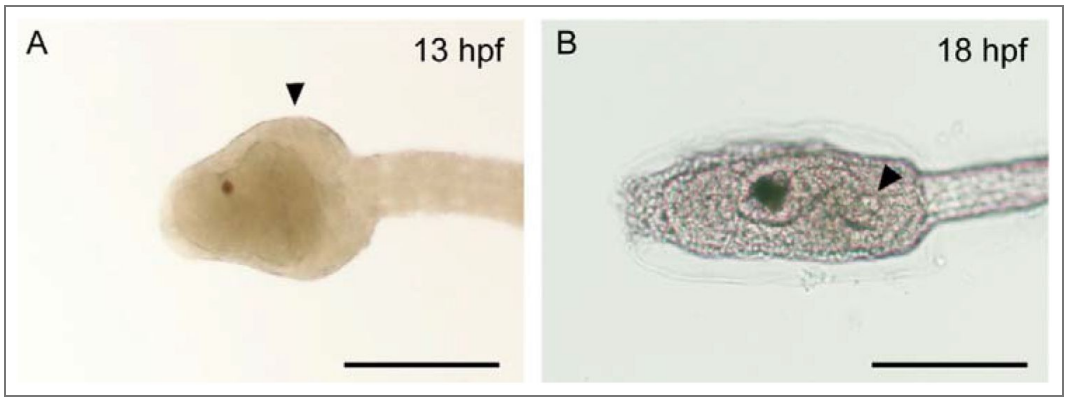

Figure 5—figure supplement 1. Entire head morphology of *Ciona* embryo.

(A, B) Bright-field images showing the entire head of *Ciona* embryos at 13 hpf and 18 hpf, illustrating how the tissue geometry becomes flatter during growth. Black arrow indicates the position of atrial siphon. Scale bar: 100 μm.

REAGENT or RESOURCE	SOURCE	IDENTIFIER
antibodies		
Phospho-Myosin Light Chain 2 (Ser19) Antibody	Cell Signaling	#3671
Alexa Fluor 647 anti-Mouse IgG	Invitrogen	#A28181
Chemicals		
EdU Cell Proliferation Kit with AF555	BeyoClick	C0075S
Alexa Fluor™ 488 Phalloidin	Thermo fisher	A12379
Protease E	sigma-Aldrich	P5147
Sodium thioglycolate	sigma-Aldrich	T0632
D-mannitol	sigma-Aldrich	M4125
MS-222	sigma-Aldrich	E10521
VECTASHIELD® with DAPI	Vectorlabs	H1200
Phanta Max Super-Fidelity DNA Polymerase	Vazyme	P505
ClonExpress MultiS One Step Cloning Kit	Vazyme	C113
TUNEL BrightRed Apoptosis Detection Kit	Vazyme	A113
Plasmids		
Epi1> MRLC::mCherry	This study	N/A
Epi1> MRLC(T18AS19A)::mCherry		N/A
Epi1> MRLC(T18ES19E)::mCherry		N/A
Epi1>PP1c::MYPT169::BcLOV4::mCherry::NES		N/A
Epi1>PP1c::MYPT169::mCherry::NES		N/A
Software		
ImageJ	NIH Image	https://imagej.nih.gov/ij/
Prism 10 CN	Graphpad Software	https://www.graphpad.com/
Imaris 10	Oxford Instruments	https://imaris.oxinst.com/
MATLAB R2021a	MathWorks	https://www.mathworks.com/

Appendix 1—table 1. **Key resource table**

Construct name	Primers	Sequence (5'→3')
MRLC	Forward	ATGTCG-AGCCGACGAACTAAA
	Reverse	CTAAATGTCATCTTTTTCTTTAGCG
MRLC(T18AS19A)	Forward	TGCAGCCGCCAATGTCTTTGCTATGTTCGATCAAGC
	Reverse	GACATTGGCGGCTGCACGCTGGGCGCGC
MRLC(T18ES19E)	Forward	TGCAGAAGAAAATGTCTTTGCTATGTTCGATCAAGCT
	Reverse	AGACATTTTCTTCTGCACGCTGGGCGCG
BcLOV4	Forward	ATGGCCACAGACGCAATCG
	Reverse	GATTATGATCTAGAGTC
PP1c	Forward	ATGGCGGACGGGGAGC
	Reverse	CCTTTTCTTCGGCGGA
MYPT169	Forward	ATGAAGATGGCGGACGCG
	Reverse	AGCTGCTTCTATATCAACCCCTTG

Appendix 1—table 2. **Primer sequences used in this study**

Acknowledgements

We are grateful to all members of the Fang Zongxi center in OUC for helpful discussions.

Additional information

Author contributions

B.D., B.L. J.Q., P.Y. conceived of the study; B.D., J.Q., P.Y., B.L., H.P., and W.S. analyzed data; P.Y. and B.L. designed the vertex model; B.D., J.Q., P.Y. and B.L. wrote the original draft. All authors approved the final version of the article.

Funding

This work was supported by the Science & Technology Innovation Project of Laoshan Laboratory (Nos. LSKJ202203204), and the Taishan Scholar Program of Shandong Province, China (B.D.).

Funding

Funder	Grant reference number	Author
The Science & Technology Innovation Project of Laoshan Laboratory	LSKJ202203204	Bo Dong

Author ORCID iDs

Bo Dong: https://orcid.org/0000-0003-1616-5363

Additional files

Figure 4—video 1. The developmental processes of the MLCP control group under blue light illumination for 1 h. Scale bar: 10 μm.

Figure 4—video 2. The developmental processes of MLCP-BcLOV4-expressed group under blue light illumination for 1 h. Scale bar: 10 μm.

Figure 5—video 1.

References

Berlew E E, Kuznetsov I A, Yamada K, Bugaj L J, Boerckel J D, Chow B Y (2021) Single-component optogenetic tools for inducible RhoA GTPase signaling. *Advanced Biology* **5**:e2100810 https://doi.org/10.1002/adbi.202100810 | PubMed

Berlew E E, Kuznetsov I A, Yamada K, Bugaj L J, Chow B Y (2020) Optogenetic Rac1 engineered from membrane lipid-binding RGS-LOV for inducible lamellipodia formation. *Photochemical and Photobiological Sciences* **19**:353-361 https://doi.org/10.1039/c9pp00434c | PubMed

Berlew E E, Yamada K, Kuznetsov I A, Rand E A, Ochs C C, Jaber Z, Gardner K H, Chow B Y (2022) Designing single-component optogenetic membrane recruitment systems: The Rho-Family GTPase signaling toolbox. *ACS Synthetic Biology* **11**:515-521 https://doi.org/10.1021/acssynbio.1c00604 | PubMed

Blair J E, Hedges S B (2005) Molecular phylogeny and divergence times of deuterostome animals. *Molecular Biology and Eevolution* **22**:2275-2284 https://doi.org/10.1093/molbev/msi225 | PubMed

Brodland G W, Conte V, Cranston P G, Veldhuis J, Narasimhan S, Hutson M S, Jacinto A, Ulrich F, Baum B, Miodownik M (2010) Video force microscopy reveals the mechanics of ventral furrow invagination. *Drosophila* **107**:22111-22116 https://doi.org/10.1073/pnas.1006591107 | PubMed

Chan C J, Heisenberg C P, Hiiragi T (2017) Coordination of morphogenesis and cell-fate specification in development. *Current Biology* **27**:R1024-r1035 https://doi.org/10.1016/j.cub.2017.07.010 | PubMed

Chiba S, Sasaki A, Nakayama A, Takamura K, Satoh N (2004) Development of Ciona intestinalis juveniles (through 2nd ascidian stage). *Zoological Science* **21**:285-298 https://doi.org/10.2108/zsj.21.285 | PubMed

Christiaen L, Wagner E, Shi W, Levine M (2009) Electroporation of transgenic DNAs in the sea squirt Ciona. *Cold Spring Harbor Protocols* **2009**:pdb.prot5345 https://doi.org/10.1101/pdb.prot5345 | PubMed

Chung S, Kim S, Andrew D J (2017) Uncoupling apical constriction from tissue invagination. *eLife* **6**:e22235 https://doi.org/10.7554/eLife.22235 | PubMed

Collinet C, Lecuit T (2021) Programmed and self-organized flow of information during morphogenesis. *Nature Reviews Molecular Cell Biology* **22**:245-265 https://doi.org/10.1038/s41580-020-00318-6 | PubMed

Conte V, Ulrich F, Baum B, Muñoz J, Veldhuis J, Brodland W, Miodownik M (2012) A biomechanical analysis of ventral furrow formation in the Drosophila melanogaster embryo. *PLOS One* **7**:e34473 https://doi.org/10.1371/journal.pone.0034473

Delsuc F, Brinkmann H, Chourrout D, Philippe H (2006) Tunicates and not cephalochordates are the closest living relatives of vertebrates. *Nature* **439**:965-968 https://doi.org/10.1038/nature04336 | PubMed

Denker E, Sehring I M, Dong B, Audisso J, Mathiesen B, Jiang D (2015) Regulation by a TGFβ-ROCK-actomyosin axis secures a non-linear lumen expansion that is essential for tubulogenesis. *Development* **142**:1639-1650 https://doi.org/10.1242/dev.117150 | PubMed

Dong B, Deng W, Jiang D (2011) Distinct cytoskeleton populations and extensive crosstalk control Ciona notochord tubulogenesis. *Development* **138**:1631-1641 https://doi.org/10.1242/dev.057208 | PubMed

Espinoza-Fonseca L M, Colson B A, Thomas D D (2014) Effects of pseudophosphorylation mutants on the structural dynamics of smooth muscle myosin regulatory light chain. *Molecular Biosystems* **10**:2693-2698 https://doi.org/10.1039/c4mb00364k | PubMed

Even-Ram S, Doyle A D, Conti M A, Matsumoto K, Adelstein R S, Yamada K M (2007) Myosin IIA regulates cell motility and actomyosin-microtubule crosstalk. *Nature Cell Biology* **9**:299-309 https://doi.org/10.1038/ncb1540 | PubMed

Fiuza U-M, Lemaire P (2021) Mechanical and genetic control of ascidian endoderm invagination during gastrulation. *Seminars in Cell and Developmental Biology* **120**:108-118 https://doi.org/10.1016/j.semcdb.2021.08.001 | PubMed

Fristrom D (1988) The cellular basis of epithelial morphogenesis. A review. *Tissue and Cell* **20**:645-690 https://doi.org/10.1016/0040-8166(88)90015-8 | PubMed

Glantz S T, Berlew E E, Chow B Y (2019) Synthetic cell-like membrane interfaces for probing dynamic protein-lipid interactions. *Methods in Enzymology* **622**:249-270 https://doi.org/10.1016/bs.mie.2019.02.015 | PubMed

Glantz S T, Berlew E E, Jaber Z, Schuster B S, Gardner K H, Chow B Y (2018) Directly light-regulated binding of RGS-LOV photoreceptors to anionic membrane phospholipids. *Proceedings of the National Academy of Sciences of the United States of America* **115**:E7720-e7727 https://doi.org/10.1073/pnas.1802832115 | PubMed

Guo H, Huang S, He B (2022) Evidence for a Role of the Lateral Ectoderm in Drosophila Mesoderm Invagination. *Front Cell Dev Biol* **10**:867438 https://doi.org/10.3389/fcell.2022.867438

Hashimoto H, Munro E (2019) Differential expression of a classic cadherin directs tissue-level contractile asymmetry during neural tube closure. *Developmental Cell* **51**:158-172.e154 https://doi.org/10.1016/j.devcel.2019.10.001 | PubMed

Hashimoto H, Robin F B, Sherrard K M, Munro E M (2015) Sequential contraction and exchange of apical junctions drives zippering and neural tube closure in a simple chordate. *Developmental Cell* **32**:241-255 https://doi.org/10.1016/j.devcel.2014.12.017 | PubMed

Hirashima T, Matsuda M (2024) ERK-mediated curvature feedback regulates branching morphogenesis in lung epithelial tissue. *Current biology : CB* **34**:683-696.e686 https://doi.org/10.1016/j.cub.2023.12.049 | PubMed

Hotta K, Dauga D, Manni L (2020) The ontology of the anatomy and development of the solitary ascidian Ciona: the swimming larva and its metamorphosis. *Scientific Reports* **10**:17916 https://doi.org/10.1038/s41598-020-73544-9 | PubMed

Hotta K, Mitsuhara K, Takahashi H, Inaba K, Oka K, Gojobori T, Ikeo K (2007) A web-based interactive developmental table for the ascidian Ciona intestinalis, including 3D real-image embryo reconstructions: I. From fertilized egg to hatching larva. *Developmental Dynamics* **236**:1790-1805 https://doi.org/10.1002/dvdy.21188 | PubMed

Iwasaki T, Murata-Hori M, Ishitobi S, Hosoya H (2001) Diphosphorylated MRLC is required for organization of stress fibers in interphase cells and the contractile ring in dividing cells. *Cell Structure and Function* **26**:677-683 https://doi.org/10.1247/csf.26.677 | PubMed

Jin P, Jan L Y, Jan Y N (2020) Mechanosensitive ion channels: structural features relevant to mechanotransduction mechanisms. *Annual Review of Neuroscience* **43**:207-229 https://doi.org/10.1146/annurev-neuro-070918-050509 | PubMed

Kiehart D P (2015) Epithelial morphogenesis: apoptotic forces drive cell shape changes. *Developmental Cell* **32**:532-533 https://doi.org/10.1016/j.devcel.2015.02.020 | PubMed

Kondo T, Hayashi S (2013) Mitotic cell rounding accelerates epithelial invagination. *Nature* **494**:125-129 https://doi.org/10.1038/nature11792 | PubMed

Kourakis M J, Newman-Smith E, Smith W C (2010) Key steps in the morphogenesis of a cranial placode in an invertebrate chordate, the tunicate Ciona savignyi. *Developmental Biology* **340**:134-144 https://doi.org/10.1016/j.ydbio.2010.01.016 | PubMed

Lecuit T, Lenne P F, Munro E (2011) Force generation, transmission, and integration during cell and tissue morphogenesis. *Annual Review of Cell and Developmental Biology* **27**:157-184 https://doi.org/10.1146/annurev-cellbio-100109-104027 | PubMed

Lee J Y, Harland R M (2007) Actomyosin contractility and microtubules drive apical constriction in Xenopus bottle cells. *Developmental Biology* **311**:40-52 https://doi.org/10.1016/j.ydbio.2007.08.010 | PubMed

Lu Q, Gao Y, Fu Y, Peng H, Shi W, Li B, Lv Z, Feng X Q, Dong B (2020) Ciona embryonic tail bending is driven by asymmetrical notochord contractility and coordinated by epithelial proliferation. *Development* **147**:dev185868 https://doi.org/10.1242/dev.185868 | PubMed

Manjón C, Sánchez-Herrero E, Suzanne M (2007) Sharp boundaries of Dpp signalling trigger local cell death required for Drosophila leg morphogenesis. *Nature Cell Biology* **9**:57-63 https://doi.org/10.1038/ncb1518 | PubMed

Martin K, Reimann A, Fritz R D, Ryu H, Jeon N L, Pertz O (2016) Spatio-temporal co-ordination of RhoA, Rac1 and Cdc42 activation during prototypical edge protrusion and retraction dynamics. *Scientific Reports* **6**:21901 https://doi.org/10.1038/srep21901 | PubMed

Matter K, Balda M S (2003) Functional analysis of tight junctions. *Methods* **30**:228-234 https://doi.org/10.1016/s1046-2023(03)00029-x | PubMed

Monier B, Gettings M, Gay G, Mangeat T, Schott S, Guarner A, Suzanne M (2015) Apico-basal forces exerted by apoptotic cells drive epithelium folding. *Nature* **518**:245-248 https://doi.org/10.1038/nature14152 | PubMed

Nagafuchi A (2001) Molecular architecture of adherens junctions. *Current Opinion in Cell Biology* **13**:600-603 https://doi.org/10.1016/s0955-0674(00)00257-x | PubMed

Nishimura M, Inoue Y, Hayashi S (2007) A wave of EGFR signaling determines cell alignment and intercalation in the Drosophila tracheal placode. *Development* **134**:4273-4282 https://doi.org/10.1242/dev.010397 | PubMed

Osswald M, Barros-Carvalho A, Carmo A M, Loyer N, Gracio P C, Sunkel C E, Homem C C F, Januschke J, Morais-de-Sá E (2022) aPKC regulates apical constriction to prevent tissue rupture in the Drosophila follicular epithelium. *Current Biology* **32**:4411-4427.e4418 https://doi.org/10.1016/j.cub.2022.08.063 | PubMed

Pearl E J, Li J, Green J B (2017) Cellular systems for epithelial invagination. *Philosophical Transactions of the Royal Society of London. Series B, Biological Sciences* **372**:20150526 https://doi.org/10.1098/rstb.2015.0526 | PubMed

Peng H, Qiao R, Dong B (2020) Polarity establishment and maintenance in ascidian notochord. *Frontiers in Cell and Developmental Biology* **8**:597446 https://doi.org/10.3389/fcell.2020.597446 | PubMed

Polyakov O, He B, Swan M, Shaevitz J W, Kaschube M, Wieschaus E (2014) Passive mechanical forces control cell-shape change during Drosophila ventral furrow formation. *Biophysical journal* **107**:998-1010 https://doi.org/10.1016/j.bpj.2014.07.013 | PubMed

Popkova A, Andrenšek U, Pagnotta S, Ziherl P, Krajnc M, Rauzi M (2024) A mechanical wave travels along a genetic guide to drive the formation of an epithelial furrow during Drosophila gastrulation. *Developmental Cell* **59**:400-414.e405 https://doi.org/10.1016/j.devcel.2023.12.016 | PubMed

Qiao J, Peng H, Dong B (2023) Development and application of an optogenetic manipulation system to suppress actomyosin activity in Ciona epidermis. *International Journal of Molecular Sciences* **24**:5707 https://doi.org/10.3390/ijms24065707 | PubMed

Schottenfeld J, Song Y, Ghabrial A S (2010) Tube continued: morphogenesis of the Drosophila tracheal system. *Current Opinion in Cell Biology* **22**:633-639 https://doi.org/10.1016/j.ceb.2010.07.016 | PubMed

Sherrard K, Robin F, Lemaire P, Munro E (2010) Sequential activation of apical and basolateral contractility drives ascidian endoderm invagination. *Current Biology* **20**:1499-1510 https://doi.org/10.1016/j.cub.2010.06.075 | PubMed

Shi W, Duclut C, Xu Y, Ma Y, Qiao J, Lin B, Yang D, Prost J, Dong B (2025) Physics of notochord tube expansion in ascidians. *Proceedings of the National Academy of Sciences of the United States of America* **122**:e2419960122 https://doi.org/10.1073/pnas.2419960122 | PubMed

Štorgel N, Krajnc M, Mrak P, trus J, Ziherl P (2016) Quantitative morphology of epithelial folds. *Biophysical Journal* **110**:269-277 https://doi.org/10.1016/j.bpj.2015.11.024 | PubMed

Sui L, Alt S, Weigert M, Dye N, Eaton S, Jug F, Myers E W, Jülicher F, Salbreux G, Dahmann C (2018) Differential lateral and basal tension drive folding of Drosophila wing discs through two distinct mechanisms. *Nature Communications* **9**:4620 https://doi.org/10.1038/s41467-018-06497-3 | PubMed

Tepass U (2002) Adherens junctions: new insight into assembly, modulation and function. *Bioessays* **24**:690-695 https://doi.org/10.1002/bies.10129 | PubMed

Vicente-Manzanares M, Ma X, Adelstein R S, Horwitz A R (2009) Non-muscle myosin II takes centre stage in cell adhesion and migration. *Nature Reviews Molecular Cell Biology* **10**:778-790 https://doi.org/10.1038/nrm2786 | PubMed

Wyatt T P J, Fouchard J, Lisica A, Khalilgharibi N, Baum B, Recho P, Kabla A J, Charras G T (2020) Actomyosin controls planarity and folding of epithelia in response to compression. *Nature materials* **19**:109-117 https://doi.org/10.1038/s41563-019-0461-x | PubMed

Yamamoto K, Miura H, Ishida M, Mii Y, Kinoshita N, Takada S, Ueno N, Sawai S, Kondo Y, Aoki K (2021) Optogenetic relaxation of actomyosin contractility uncovers mechanistic roles of cortical tension during cytokinesis. *Nature Communications* **12**:7145 https://doi.org/10.1038/s41467-021-27458-3 | PubMed

Zartman J J, Shvartsman S Y (2010) Unit operations of tissue development: epithelial folding. *Annual Review of Chemical and Biomolecular Engineering* **1**:231-246 https://doi.org/10.1146/annurev-chembioeng-073009-100919 | PubMed

Zhao L, Gao F, Gao S, Liang Y, Long H, Lv Z, Su Y, Ye N, Zhang L, Zhao C, *et al.* (2021) Biodiversity-based development and evolution: the emerging research systems in model and non-model organisms. *Science China. Life Sciences* **64**:1236-1280 https://doi.org/10.1007/s11427-020-1915-y | PubMed

Peer reviews

Reviewer #1 (Public review):

Summary:

This paper investigates the physical basis of epithelial invagination in the morphogenesis of the ascidian siphon tube. The authors observe changes in actin and myosin distribution during siphon tube morphogenesis using fixed specimens and immunohistochemistry. They discover that there is a biphasic change in the actomyosin localization that correlates with changes in cell shapes. Initially, there is the well-known relocation of actomyosin from the lateral sides to the apical surface of cells that will invaginate, accompanied by a concomitant lengthening of the central cells within the invagination, but not a lot of invagination. Coincident with a second, more rapid, phase of invagination, the authors see a relocalization of actomyosin back to the lateral sides of the cells. This 2nd "bidirectional" relocation of actin appears to be important because optogenetic inhibition of myosin in the lateral domain after the initial invaginations phase resulted in a block of further invagination. Although not noted in the paper, that the second phase of siphon invagination is dependent on actomyosin is interesting and important because it has been shown that during Drosophila mesoderm invagination that a second "folding" phase of invagination is independent of actomyosin contraction (Guo et al. eLife 2022), so there appear to be important differences between the Drosophila mesoderm system and the ascidian siphon tube systems.

Using the experimental data, the authors create a vertex model of the invagination, and simulations reveal a coupled mechanism of apicobasal tension imbalance and lateral contraction that creates the invagination. The resultant model appears to recapitulate many aspects of the observed cell behaviors, although there are some caveats to consider (described below).

Strengths:

The studies and presented results are well done and provide important insights into the physical forces of epithelial invagination, which is important because invaginations are how a large fraction of organs in multicellular organisms are formed.

Weaknesses:

(1) This reviewer has concerns about two aspects of the computational model. First, the model in Fig. 5D shows a simulation of a flat epithelial sheet creating an invagination. However, the actual invagination is occurring in a small embryo that has significant curvature, such that nine or so cells occupy a 90-degree arc of the 360-degree circle that defines the embryo's cross-section (e.g., see Fig. 1A). This curvature could have important effects on cell behavior.

(2) The second concern about the model is that Figure 5 D shows the vertex model developing significant "puckering" (bulging) surrounding the invagination. Such "puckering" is not seen in the in vivo invagination (Fig. 1A, 2A). This issue is not discussed in the text, so it is unclear how big an issue this is for the developed model, but the model does not recapitulate all aspects of the siphon invagination system.

(3) In Fig. 2A Top View and the schematic in Fig. 2C, the developing invagination is surrounded by a ring of aligned cell edges characteristic of a "purse string" type actomyosin cable that would create pressure on the invaginating cells that has been documented in multiple systems. Notably, the schematic in Fig 2C shows myosin II localizing to aligned "purse string" edges, suggesting the purse string is actively compressing the more central cells. If the purse string consistently appears during siphon invagination, a complete understanding of siphon invagination will require understanding the contributions of the purse string to the invagination process.

(4) The introduction and discussion put the work in context of work on physical forces in invagination, but there is not much discussion of how the modeling fits into the literature.

Comment on revised version.

This is an extensively revised version of a previously submitted manuscript that, as detailed in their 20-page response to the first reviews, satisfactorily addresses the reviewers' comments. In particular, the revised manuscript makes it much clearer how this work fits into and advances the field. The added experiments strengthen the rigor of the manuscript as well. Overall, this paper is ready to go.

https://doi.org/10.7554/eLife.108588.2.sa3

Reviewer #2 (Public review):

Summary:

The authors propose that bidirectional redistribution of actomyosin drives tissue invagination in Ciona siphon tube formation. They suggest a two-stage model where actomyosin first accumulates apically to drive a slow initial invagination, followed by redistribution to lateral domains to accelerate the invagination process through cell shortening. They have shown that actomyosin activity is important for invagination - modulation of myosin activity through expression of myosin mutants altered the timing and speed of invagination; furthermore, optogenetic inhibition of myosin during the transition of the slow and fast stages disrupted invagination. The authors further developed a vertex model to validate the relationship between contractile force distribution and epithelial invagination.

Strengths:

(1) The authors employed various techniques to address the research question, including optogenetics, use of MRLC mutants, and vertex modelling.

(2) The authors provide quantitative analyses for a substantial portion of their imaging data, including cell and tissue geometry parameters as well as actin and myosin distributions. The sample sizes used in these analyses appear appropriate.

(3) The authors combined experimental measurements with computer modeling to test the proposed mechanical models, which represents a strength of the study. It provides a framework to explore the mechanical principles underlying the observed morphogenesis.

Comments on the revision.

The revised manuscript has been substantially improved. The authors have addressed many of my previous concerns through the addition of new data, analyses, and discussion. The characterization of epithelial folding in the ascidian Ciona provides valuable insight into a comparatively less explored morphogenetic system, and the imaging and quantitative analyses are overall compelling. That said, a few important points remain to be addressed.

One remaining issue concerns the mechanistic novelty of the actomyosin redistribution described in this study. The authors emphasize that the key novelty lies in the stepwise translocation of actomyosin from the lateral membrane to the apical domain during the initial stage (apical constriction), followed by redistribution from the apical domain back to the lateral domain during the accelerated stage (invagination). I agree that the dynamic redistribution itself is potentially interesting and may represent an underexplored aspect of epithelial morphogenesis. However, as I discussed in my previous review comments, from a mechanics perspective, the role of apical actomyosin in driving apical constriction and of lateral actomyosin in contributing to tissue folding/invagination have already been demonstrated in multiple systems, although to varying extents depending on the model. Therefore, while the current study convincingly documents a distinct spatiotemporal sequence of actomyosin localization in Ciona atrial siphon tube formation, it could be clarified further to what extent this work advances new mechanical principles underlying epithelial folding, as opposed to revealing a variation in the deployment of previously described force-generating modules.

Importantly, I think the manuscript has the potential to provide deeper conceptual insight if the authors more explicitly consider the significance of the "redistribution" process itself. Redistribution does not only involve the appearance of actomyosin at a new membrane domain; it also necessarily involves its disappearance from the previous domain. The latter aspect has, in my view, been much less explored in the literature. For example: Is the removal of lateral actomyosin during the early phase important for efficient apical constriction? Conversely, is the reduction of apical actomyosin during the later accelerated phase important for proper invagination mechanics? These questions are particularly interesting because they address whether redistribution between domains serves an active mechanical regulatory role, rather than focusing on the role of force-generating actomyosin at a given location.

I acknowledge that addressing these questions experimentally could be technically challenging. One potentially powerful way to address this would be through the revised computational model. For example, the authors could test whether tissue folding is altered when actomyosin is allowed to accumulate at a new domain without being concomitantly depleted from the original domain. Such analyses could help distinguish whether redistribution itself has functional mechanical importance, rather than merely reflecting sequential recruitment to different cellular regions. In my opinion, incorporating this aspect would substantially strengthen the conceptual and mechanistic novelty of the study.

My other concern relates to the new optogenetic data presented in Figure 4-figure supplement 2. In the "Dark" samples, active myosin does not appear to be clearly enriched along the membrane, but instead seems relatively diffuse within the cytoplasm. This appears distinct from the images shown in Figure 2, where active myosin exhibits clear membrane enrichment. Could the authors provide top-view images for the samples shown in Figure 4-figure supplement 2? This would help clarify whether active myosin is indeed enriched along the apical membrane at 16 hpf and along the lateral membrane at 17 hpf in the "Dark" condition.

In addition, the tissue morphology in the "17 hpf Light 1 hr" panel of Figure 4-figure supplement 2 appears noticeably different from that shown in Figure 4. Specifically, the apical side of the tissue in Figure 4 appears substantially more relaxed than in Figure 4-figure supplement 2. Based on the authors' interpretation of the optogenetic experiments, apical active myosin is not strongly affected by the treatment described in Figure 4. If so, one would expect apical constriction to remain largely intact. However, the more relaxed apical domain shown in Figure 4 seems to suggest that apical constriction may in fact be perturbed by the optogenetic manipulation. This apparent discrepancy complicates the interpretation of the

experiment and seems somewhat inconsistent with the authors' main conclusion from this figure.

https://doi.org/10.7554/eLife.108588.2.sa2

Reviewer #3 (Public review):

Summary:

In this revised manuscript by Qiao et al., the authors seek to uncover force and contractility dynamics that drive tissue morphogenesis, using the Ciona atrial siphon primordium as a model. Specifically, the authors perform a detailed examination of epithelial folding dynamics. Generally, the authors' claims were supported by their data, and the conceptual advances may have broader implications for other epithelial morphogenesis processes in other systems.

Strengths:

The strengths of this manuscript include the variety of experimental and theoretical methods, including generally rigorous imaging and quantitative analyses of actomyosin dynamics during this epithelial folding process, and the derivation of a mathematical model based on their empirical data, which they perturb in order to gain novel insights into the process of epithelial morphogenesis.

Weaknesses:

Concerns raised in the initial submission were addressed in the revised manuscript.

https://doi.org/10.7554/eLife.108588.2.sa1

Author response:

The following is the authors' response to the original reviews.

> ***Public Reviews:***
>
> ***Reviewer #1 (Public review):***
>
> *Summary:*
>
> *This paper investigates the physical basis of epithelial invagination in the morphogenesis of the ascidian siphon tube. The authors observe changes in actin and myosin distribution during siphon tube morphogenesis using fixed specimens and immunohistochemistry. They discover that there is a biphasic change in the actomyosin localization that correlates with changes in cell shapes. Initially, there is the well-known relocation of actomyosin from the lateral sides to the apical surface of cells that will invaginate, accompanied by a concomitant lengthening of the central cells within the invagination, but not a lot of invagination. Coincident with a second, more rapid, phase of invagination, the authors see a relocalization of actomyosin back to the lateral sides of the cells. This 2nd "bidirectional" relocation of actin appears to be important because optogenetic inhibition of myosin in the lateral domain after the initial invaginations phase resulted in a block of further invagination. Although not noted in the paper, that the second phase of siphon invagination is dependent on actomyosin is interesting and important because it has been shown that during Drosophila mesoderm invagination that a second "folding" phase of invagination is independent of actomyosin contraction (Guo et al. elife 2022), so there appear to be important differences between the Drosophila mesoderm system and the ascidian siphon tube systems.*

> *Using the experimental data, the authors create a vertex model of the invagination, and simulations reveal a coupled mechanism of apicobasal tension imbalance and lateral contraction that creates the invagination. The resultant model appears to recapitulate many aspects of the observed cell behaviors, although there are some caveats to consider (described below).*

We thank the reviewer for the insightful summary and for bringing the important study by Guo et al. (2022) to our attention. We have now added a dedicated comparison with *Drosophila* ventral furrow invagination in the Discussion, explicitly highlighting that the second rapid folding phase in *Drosophila* does not require lateral contractility, whereas in our system lateral contractility is obligatory for the accelerated invagination stage.

> *Strengths:*
>
> *The studies and presented results are well done and provide important insights into the physical forces of epithelial invagination, which is important because invaginations are how a large fraction of organs in multicellular organisms are formed.*

Thank you for this positive assessment and for recognizing the significance of our work in elucidating the physical mechanisms underlying fundamental morphogenetic processes. We have striven to provide a comprehensive and rigorous analysis, and are grateful for this encouraging feedback.

> *Weaknesses:*
>
> *(1) This reviewer has concerns about two aspects of the computational model. First, the model in Figure 5D shows a simulation of a flat epithelial sheet creating an invagination. However, the actual invagination is occurring in a small embryo that has significant curvature, such that nine or so cells occupy a 90-degree arc of the 360-degree circle that defines the embryo's cross-section (e.g., see Figure 1A). This curvature could have important effects on cell behavior.*

Thank you for bringing up the issue of tissue curvature. In the initial version of our model, we treated the tissue as flat based on the local geometry of the anterior epidermis. Although the embryo at 13 hpf indeed possesses significant curvature, its overall transverse cross-section is approximately elliptical, and the region undergoing invagination is situated in a relatively low-curvature zone, occupying only a 30° ~ 40° arc of the entire tissue. More importantly, the embryo undergoes anisotropic elongation and expansion, becoming significantly flattened during the accelerated invagination stage, eventually adopting a very flat geometry by 18 hpf. We have now included Figure 5—figure supplement 1 to clarify these global morphological transitions.

Nevertheless, the curvature does exist during the early stages, and we agree that clarifying its potential role is essential. Therefore, in the revised manuscript, we have updated our vertex model to incorporate a simplified circular geometry. Furthermore, unlike *Drosophila* ventral furrow formation (Guo et al., eLife, 2022), the invagination here eventually forms a hollow tubular structure, which led us to introduce a surface bending stiffness term into the mode. Although global tissue growth is not explicitly modeled, we explored the impact of curvature by varying the initial system size. Our results demonstrate that the invagination process, driven by apico-basal tension imbalance and lateral contraction, is highly localized and remains robust across different curvatures.

> *(2) The second concern about the model is that Figure 5 D shows the vertex model developing significant "puckering" (bulging) surrounding the invagination. Such "puckering" is not seen in the in vivo invagination (Figure 1A, 2A). This issue is not*

> *discussed in the text, so it is unclear how big an issue this is for the developed model, but the model does not recapitulate all aspects of the siphon invagination system.*

Thank you for pointing out this. In our experiments, the similar "puckering" shape is observed during the early stages of morphogenesis (~17 hpf, as seen in Figure 1A) when the tissue size is relatively small. However, this feature rapidly disappears as the tissue grows and the overall geometry becomes flatter. This suggests that "puckering" is more pronounced in highly curved epithelia, a phenomenon that aligns with mechanical expectations. Previous vertex models of *Drosophila* ventral furrow formation do not exhibit this effect (Brodland et al., 2010; Polyakov et al., 2014), because they modeled cells within a rigid unmovable boundary. However, in our system of siphon morphogenesis, a tubular structure ultimately forms in the epithelium without strong boundary constraints. Thus, the mechanical boundary conditions are basically different.

Also, the formation of a hollow tubular structure—supported by strong F-actin accumulation at the tissue surface—indicates a bending stiffness of surface tissue (Figure 1), which we have incorporated into the model. This bending term enforces smooth curvature transitions, which can manifest as a "puckering" shape surrounding the invagination. In our previous flat-geometry model, this significant bending stiffness led to a "puckering" effect surrounding the invagination. In our updated curved vertex model, this phenomenon also exists and is found to be related to tissue curvature. By simulating a larger system with low curvature (N = 324 cells in Figure 6D), we find that this puckering is significantly reduced. This confirms that the shape discrepancy is a size-dependent effect of the bending constraints within a fixed system size that did not account for tissue growth. In biological development, continuous growth and flattening of the embryo diminish this effect (Figure 5—figure supplement 1), aligning our model's predictions.

Furthermore, we note that the cell-cell adhesion between the surface epithelium and the internal bulk cells (a factor not explicitly captured in our current model) likely further suppresses such evagination *in vivo*, as outward puckering would necessitate the coordinated deformation of the underlying tissues. We aim to investigate the interplay between global growth and local active forces in future work. We have added a detailed description and mechanical explanation of these simulated shapes in the revised manuscript.

> *(3) In Figure 2A, Top View, and the schematic in Figure 2C, the developing invagination is surrounded by a ring of aligned cell edges characteristic of a "purse string" type actomyosin cable that would create pressure on the invaginating cells, which has been documented in multiple systems. Notably, the schematic in Figure 2C shows myosin II localizing to aligned "purse string" edges, suggesting the purse string is actively compressing the more central cells. If the purse string consistently appears during siphon invagination, a complete understanding of siphon invagination will require understanding the contributions of the purse string to the invagination process.*

Thank you for this excellent observation. We agree that the ring-like actomyosin structure is a prominent feature during the initial stages of invagination, and its potential role warrants discussion. We carefully re-examined our data. Our analysis confirms that this myosin ring is most pronounced during the early initial invagination stage. This inward compression from the periphery would work in concert with apical constriction to help shape the initial invagination. However, this ring-like myosin pattern significantly diminishes during the accelerated invagination stage, indicating that sustained compression from the purse string is not required for the entire process. We have added a discussion of this point in the revised manuscript. We also agree with that future experiments using laser ablation or optogenetic inhibition specifically targeting this actomyosin ring would be valuable to further dissect its precise contribution during the early invagination stage, and we have noted this as a future direction in the Discussion.

> *(4) The introduction and discussion put the work in the context of work on physical forces in invagination, but there is not much discussion of how the modeling fits into the literature.*

We thank the reviewer for this suggestion. We have now incorporated additional references and discussion regarding existing theoretical models and the physical forces involved in tissue invagination. These previous studies provided the foundational framework for our updated curved vertex model. We have also added an explanation of how our model differs from these existing works and discussed potential future directions for further investigation.

> ***Reviewer #2 (Public review):***
>
> *Summary:*
>
> *The authors propose that bidirectional translocation of actomyosin drives tissue invagination in Ciona siphon tube formation. They suggest a two-stage model where actomyosin first accumulates apically to drive a slow initial invagination, followed by translocation to lateral domains to accelerate the invagination process through cell shortening. They have shown that actomyosin activity is important for invagination - modulation of myosin activity through expression of myosin mutants altered the timing and speed of invagination; furthermore, optogenetic inhibition of myosin during the transition of the slow and fast stages disrupted invagination. The authors further developed a vertex model to validate the relationship between contractile force distribution and epithelial invagination.*

Thank you for your thoughtful and accurate summary of our work and for your constructive critique.

> *Strengths:*
>
> *(1) The authors employed various techniques to address the research question, including optogenetics, the use of MRLC mutants, and vertex modelling.*
>
> *(2) The authors provide quantitative analyses for a substantial portion of their imaging data, including cell and tissue geometry parameters as well as actin and myosin distributions. The sample sizes used in these analyses appear appropriate.*
>
> *(3) The authors combined experimental measurements with computer modeling to test the proposed mechanical models, which represents a strength of the study. It provides a framework to explore the mechanical principles underlying the observed morphogenesis.*

We are grateful for your positive assessment of the multidisciplinary approaches, quantitative analyses, and the integration of modeling with experiments.

> *Weaknesses:*
>
> *(1) The concept of coordinated and sequential action of apical and lateral actomyosin in support of epithelial folding has been documented through a combination of experimental and modeling approaches in other contexts, such as ascidian endoderm invagination (PMID: 20691592) and gastrulation in Drosophila (PMIDs: 21127270, 22511944, 31273212). While the manuscript addresses an important question, related findings have been reported in these previous studies. This overlap reduces the degree of novelty, and it remains to be clarified how their work advances beyond these prior contributions.*

We thank the reviewer for raising this important point. In the revised Introduction and Discussion, we have explicitly distinguished our findings from prior studies. Specifically: (1)

Unlike ascidian endoderm invagination, where actomyosin shifts from apical to basolateral (Sherrard et al., 2010), our system exhibits a bidirectional redistribution between apical and lateral domains, with the basal domain playing a passive role. (2) Unlike *Drosophila* ventral furrow invagination, where lateral contractility is not essential for the second folding phase (Guo et al., 2022), our optogenetic inhibition demonstrates that lateral contractility is obligatory for the accelerated invagination stage. These comparisons, now clearly stated in the Introduction and Discussion, establish bidirectional actomyosin redistribution as a distinct mechanical paradigm for sequential morphogenesis. We believe these revisions adequately clarify how our work advances beyond prior contributions.

> *(2) One of the central statements made by the authors is that the translocation of actomyosin between the apical and lateral domains mediates invagination. The use of the term "translocation" infers that the same actomyosin structures physically move from one location to another location, which is not demonstrated by the data. Given the time scale of the process (several hours), it is also possible that the observed spatiotemporal patterns of actomyosin intensity result from sequential activation/assembly and inactivation/disassembly at specific locations on the cell cortex, rather than from the physical translocation of actomyosin structures over time.*

We thank the reviewer for this important point. We agree that our data do not demonstrate physical translocation of actomyosin structures, and that the observed patterns could arise from sequential assembly/disassembly over time. To avoid overinterpretation, we have replaced “translocation” with “redistribution” throughout the manuscript (including the title) and toned down the language in the Results and Discussion.

> *(3) Some aspects of the data on actomyosin localization require further clarification. (1) The authors state that actomyosin translocation is bidirectional, first moving from the lateral domain to the apical domain; however, the reduction of the lateral actomyosin at this step was not rigorously tested. (2) During the slow invagination stage, it is unclear whether myosin consistently localizes to the apical cell-cell borders or instead relocalizes to the medioapical domain, as suggested by the schematic illustration presented in Figure 2C. (3) It is unclear how many cells along the axis orthogonal to the furrow accumulate apical and lateral myosin.*

Thank you for your insightful comments, which will help us significantly improve the clarity and rigor of our actomyosin localization analysis. To address the points raised, we undertake several key revisions: First, we have added new quantitative analyses of active myosin intensity from earlier time points (14-15 hpf) to rigorously support the initial lateral-to-apical redistribution phase (Figure 2B). Second, the schematic in Figure 2C has been corrected to show myosin at the apical cell-cell borders. We have clarified that redistribution occurs in a domain of approximately 15-20 cells (the invagination primordium), not only the center cell.

> *(4) The overexpression of MRLC mutants appears to be rather patchy in some cases (e.g., in Figure 3A, 17.0 hpf, only cells located at the right side of the furrow appeared to express MRLC T18ES19E). It is unclear how such patchy expression would impact the phenotype.*

Thank you for your observation. We acknowledge that mosaic expression is common in *Ciona* electroporation. For all quantitative analyses, we only selected embryos in which the central cell, along with more than half of the surrounding cells in the primordium, showed clear expression of the plasmid. This selection criterion has been added to the Materials and Methods section.

> *(5) In the optogenetic experiment, it appears that after one hour of light stimulation, the apical side of the tissue underwent relaxation (comparing 17 hpf and 16 hpf in Figure 4B). It is therefore unclear whether the observed defect in invagination is due to apical*

> *relaxation or lack of lateral contractility, or both. Therefore, the phenotype is not sufficient to support the authors' statement that "redistribution of myosin contractility from the apical to lateral regions is essential for the development of invagination".*

We have performed the additional immunostaining experiment of myosin II. The new data (Figure 4—figure supplement 2) showed that light stimulation specifically reduced lateral myosin intensity without significantly affecting apical myosin compared to the dark control. Therefore, the observed block of invagination is primarily due to loss of lateral contractility.

> *(6) The vertex model is designed to explore how apical and lateral tensions contribute to distinct morphological outcomes. While the authors raise several interesting predictions, these are not further tested, making it unclear to what extent the model provides new insights that can be validated experimentally. In addition, modeling the epithelium as a flat sheet and not accounting for cell curvature is a simplification that may limit the model's accuracy. Finally, the model does not fully recapitulate the deeply invaginated furrow configuration as observed in a real embryo (comparing 18 hpf in Figure 5D and 18 hpf in Figure 1A) and does not fully capture certain mutant phenotypes (comparing 18 hpf in Figure 5F and 18 hpf in Figure 3B right panel).*

Thank you very much for these helpful and constructive comments. We have addressed your concerns through the following model updates and clarifications.

First, we have reformulated our vertex model from a flat sheet to a curved geometry that incorporates initial tissue curvature. We found that the core mechanical mechanism, mediated by the coupling of apical and lateral active contraction, consistently recapitulates the experimental invagination process. By independently inhibiting apical or lateral contractions in the model, we further clarified their distinct mechanical contributions to tissue bending and cell shortening.

Regarding the model predictions concerning the apical-to-lateral redistribution of actomyosin in the original version (previously shown in Figure 6E-H), we agree that these lacked direct experimental validation in the current study and may have strayed from the primary focus on the invagination mechanism itself. Therefore, we have removed these predictive components from the revised manuscript. Instead, we have refocused our analysis on the robustness of the localized active process across tissues of varying sizes and curvatures, particularly because the *in vivo* invagination is accompanied by global tissue growth and geometry changes.

Finally, we acknowledge that the simulated final shapes do not perfectly match the experimental geometry in every detail. We attribute these discrepancies to the omission of global tissue growth and the simplification of cell-cell adhesions between the surface epithelium and internal bulk cells. While these factors are not the primary drivers of the invagination, they undoubtedly refine the local morphology. We have added discussions of these limitations in the revised manuscript and aim to incorporate precise experimental measurements of tissue growth and inter-layer interactions in future modeling efforts.

> ***Reviewer #3 (Public review):***
>
> *Summary:*
>
> *In this manuscript by Qiao et al., the authors seek to uncover force and contractility dynamics that drive tissue morphogenesis, using the Ciona atrial siphon primordium as a model. Specifically, the authors perform a detailed examination of epithelial folding dynamics. Generally, the authors' claims were supported by their data, and the conceptual advances may have broader implications for other epithelial morphogenesis processes in other systems.*

Thank you for your positive summary and for recognizing the broader implications of our work.

> *Strengths:*
>
> *The strengths of this manuscript include the variety of experimental and theoretical methods, including generally rigorous imaging and quantitative analyses of actomyosin dynamics during this epithelial folding process, and the derivation of a mathematical model based on their empirical data, which they perturb in order to gain novel insights into the process of epithelial morphogenesis.*

Thank you for highlighting the strengths of our multidisciplinary methodology.

> *Weaknesses:*
>
> *There are concerns related to wording and interpretations of results, as well as some missing descriptions and details regarding experimental methods.*

We have revised the manuscript to address your concerns regarding the wording and the details of the methodology.

> ***Recommendations for the authors:***
>
> ***Reviewing Editor Comments:***
>
> *Based on the feedback from the reviewers, a focus on the following major points has the potential to improve the overall assessment of the significance of the findings and the strength of the evidence:*
>
> *(1) It would be helpful to clearly articulate how these findings advance the field beyond what has already been demonstrated or suggested in other systems.*

We thank the editor for this helpful suggestion. To better articulate how our findings advance the field, we have revised both the Introduction and Discussion to explicitly contrast our system with previously studied invagination models. Specifically, we highlight that our work demonstrates a bidirectional redistribution of actomyosin between apical and lateral domains, which differs from the apical-to-basolateral shift reported in ascidian endoderm invagination. Moreover, we emphasize that lateral contractility is obligatory for the accelerated invagination stage in our system, whereas in *Drosophila* ventral furrow invagination the second folding phase can proceed without it. These comparisons have been clearly presented in the revised manuscript. We think our findings represent a distinct mechanical paradigm for sequential epithelial morphogenesis.

> *(2) It would be helpful to clarify the meaning of "translocation" and more explicitly describe the temporal and spatial patterns of active myosin localization during the two steps of invagination.*

We have replaced the term “translocation” with “redistribution” throughout the manuscript, including the title. We have also added new quantitative analyses of active myosin intensity from earlier time points (14–15 hpf) to rigorously support the initial lateral-to-apical redistribution phase (Figure 2B). High-resolution top-view images have been included to show the ring-like localization of myosin at the apical cell-cell junctions during the initial stage (Figure 2A). The schematic in Figure 2C has been corrected to accurately reflect the predominant localization of active myosin at the apical cell-cell borders.

> *(3) It would be helpful to explain how the optogenetic data support the conclusion that "redistribution of myosin contractility from the apical to lateral regions is essential for the development of invagination".*

We have performed additional experiments combining optogenetic inhibition with subsequent immunostaining of active myosin II (anti-pS19 MRLC). We quantitatively compared the distribution of actomyosin in light-stimulated versus dark-control embryos. The new data show that after light exposure, lateral myosin intensity is significantly reduced compared to the dark control, whereas apical myosin levels decrease similarly in both groups. This indicates that the optogenetic manipulation effectively attenuates lateral contractility during the accelerated invagination stage without affecting concurrent apical contractility changes. These results directly support the conclusion that lateral contractility acquisition is essential for invagination progression. (Figure 4—figure supplement 2)

> *(4) It would be helpful to describe how the modeling work fits within the existing literature on modeling epithelial folding and to address discrepancies between the model and the actual biological observations, such as tissue curvature, limited invagination depth in the model, and the "puckering" surrounding the invagination. In addition, certain descriptions of the modeling results should be clarified, as suggested by Reviewer #3.*

We thank the referees for the detailed and constructive comments on our modeling work. In response to these suggestions, we have significantly updated the theoretical section of the manuscript. Specifically, we have reformulated the vertex model within a curved geometry that represents the entire tissue, and revised the subsequent analyses to better clarify the mechanical principles driving the observed morphogenesis. We have added relevant references and discussed the mechanistic connections and distinctions between our model and previous studies on epithelial invagination. We hope that our point-by-point responses of the modeling work and the corresponding revisions in the manuscript adequately address the reviewers' concerns.

> *(5) It would be helpful to elaborate on the methods for quantitative image analysis and statistical tests.*

We have thoroughly expanded the Materials and Methods section by adding a dedicated subsection "Quantification and statistical analysis". This subsection provides step-by-step descriptions of how apical, lateral, and basal domains were defined (segmented line, width 1 μm), how normalization was performed (basal intensity set to 1), how center cell height, invagination depth, and lateral cell distance were measured (referencing Figure 1B), and what statistical tests were used (two-tailed Student's t-test, with significance levels indicated). (see revised Materials and Methods, "Quantification and statistical analysis" subsection)

> ***Reviewer #1 (Recommendations for the authors):***
>
> *(1) This reviewer has concerns about two aspects of the model. First, the model in Figure 5D shows a simulation of a flat epithelial sheet creating an invagination. However, the actual invagination is occurring in a small embryo that has very significant curvature, such that nine or so cells occupy a 90-degree arc of the 360-degree circle that defines the embryo's section (e.g., see Figure 1A). This curvature could potentially have important effects on cell behavior. Ideally, the developed model would reflect the actual geometry of the observed behavior. A more nuanced analysis would provide important insight into whether the embryo's curvature makes a difference. Importantly, any result comparing the planar versus curved system would be interesting because if the model worked equally well in the high curvature or planar systems, the model is robust, or if invagination requires different strategies for high curvature and for planar systems, this*

> *is an important finding that reveals the importance of local geometries. I don't think the consideration of invagination from a planar vs curved epithelium has been previously modeled.*

We fully agree with the reviewer that comparing planar versus curved systems provides valuable insights into the invagination mechanism. As we addressed in our response to Reviewer #1 (Public Review) - Weakness (1), we have now updated our vertex model to incorporate curved geometries and introduced surface bending stiffness to better reflect the embryo's actual shape. Our systematic comparison reveals that the invagination process, driven by apico-basal tension imbalance and lateral contraction, is indeed highly localized and remains robust across different initial curvatures. We have added Figure 5—figure supplement 1 and corresponding discussions in the revised manuscript to highlight these findings on model robustness and the role of local geometry.

> *(2) The second concern about the model is that Figure 5D shows the vertex model developing significant "puckering" (evagination) surrounding the invagination. Such "puckering" is not seen in the in vivo invagination (Figures 1A, 2A). This issue is not discussed in the text, so it is unclear how big an issue this is for the developed model. A discussion of this issue in the text would be appropriate. Maybe puckering goes away if a curved epithelium is modeled?*

Thank you for this comment. In our model, the "puckering" effect naturally arises due to the presence of surface bending stiffness and the absence of rigid boundary constraints, which resembles the tissue morphology observed at 17 hpf in our experiments. However, our updated simulations show that this effect significantly diminishes as the tissue curvature decreases. We have addressed this concern in detail in our response to Reviewer #1 (Public Review) - Weakness (2) and have included the relevant analysis and discussions in the revised manuscript.

> *(3) Because of the puckering, it is unclear in the model what measurement is being used to define the invagination depth in Figure 5E. Is the depth from the maximal height of the surrounding epithelial cells? Or the location of the apical surface before invagination begins? It would be helpful to have that parameter better defined, and it would also be helpful to add a line to Figure 5D showing how the reference point for invagination depth.*

Thank you for your suggestion. We measured the vertical distance from the baseline connecting the maximal height of apical midpoints of the surrounding cells to the apical surface of the center cell, which is consistent with our experimental measurements. We have now added a schematic line and indicators to Figure 5D.

> *(4) In Figure 2A Top View, as well as the schematic in Figure 2C, the developing invagination is surrounded by a ring of aligned cell edges characteristic of a "purse string" type actomyosin cable that would create pressure on the invaginating cells, which have been documented in multiple systems. Notably, the schematic in Figure 2C shows myosin II localizing to aligned "purse string" edges, suggesting the purse string is actively compressing the more central cells. If the purse string consistently appears during siphon invagination, a complete understanding of siphon invagination will require understanding the contributions of the purse string to the invagination process. For this paper, a discussion of the possible involvement of a purse string would be helpful for the readers, but follow-up work could include laser cutting or optogenetic blockage of the purse string contractility.*

Thank you for your suggestion. We agree that the ring-like actomyosin structure is a prominent feature during the initial stages of invagination, and its potential role warrants discussion. We carefully re-examined our data. Our analysis confirms that this myosin ring is

most pronounced during the early initial invagination stage (Figure 2A). This inward compression from the periphery would work in concert with apical constriction to help shape the initial invagination. However, this ring-like myosin pattern significantly diminishes in the accelerated invagination stage. We propose that the purse string may play a collaborative role in the early phase. We agree that follow-up work (e.g., laser cutting or optogenetic manipulation) would be valuable and have noted this as a future direction in the Discussion.

> *(5) The introduction and discussion put the work in the context of work on physical forces in invagination, but there is not much discussion of how the modeling fits into the literature. Did the current work advance the state of modeling of such phenomena? What were the strengths and limitations of the modeling in this paper compared to what has been done previously?*

Thank you for this suggestion. While we have incorporated additional literature in the revised manuscript as mentioned in our response to Reviewer #1 (Public Review) - Weakness (4), we would like to further clarify the specific advances and limitations of our modeling framework. Our updated vertex model builds upon established foundational frameworks but advances the state of modeling by: (i) incorporating dynamic apico-lateral tension variations coupled with actomyosin signals, and (ii) achieving localized, activity-mediated morphogenesis without the need for external rigid boundary constraints—a feature that distinguishes it from many classical models. We also recognize the model's current limitations. Specifically, it does not explicitly account for compressive stress and global geometric changes induced by tissue growth. The mechanical interactions between surface epithelial cells and the underlying internal bulk cells are also simplified. These factors represent important directions for our future work. We have added a dedicated paragraph in the Modeling and Discussion sections to contrast our model with existing literature and to explicitly state these strengths and limitations.

> *(6) Figure 4D. Minor point, but the labeling on the X-axis is out of register with the bar graphs.*

We have corrected the alignment of the X-axis labels with the bar graphs in Figure 4D. The figure has been updated accordingly.

> *(7) Figure 4B does not have a scale bar.*

We have added a scale bar to Figure 4B (10 μm).

> ***Reviewer #2 (Recommendations for the authors):***
>
> *(1) Live imaging is necessary to demonstrate bidirectional translocation by visualizing the movement of the actomyosin network between the apical and lateral domains. Alternatively, a term other than "translocation" should be used to describe the observation.*

We agree that live imaging of actomyosin movement would be ideal but is technically challenging in this system. Instead, we have replaced the term “translocation” with the more accurate and conservative term “redistribution” throughout the manuscript, including the title, to avoid implying physical movement of the same molecules. This addresses the reviewer’s concern.

> *(2) The optogenetic tool could be used to its full potential by manipulating myosin spatially or temporally, for example, by inhibiting myosin at various stages or subcellular locations, which would provide an opportunity to thoroughly test the domain and stage-specific needs for actomyosin. That said, I recognize that such experiments may be challenging in the model system used in this study.*

We thank the reviewer for this suggestion. We have indeed attempted spatially restricted optogenetic activation in the *Ciona* atrial siphon system, but found it technically very challenging due to tissue geometry and light scattering. We appreciate the reviewer's understanding of these technical limitations.

> *(3) Some additional characterization of the optogenetics tool, such as the distribution of active myosin and F-actin post-stimulation, could further strengthen the interpretation of the inhibitory effect on invagination.*

We thank the reviewer for this suggestion. After optogenetic inhibition, we fixed and stained embryos for active myosin II. The results (Figure 4—figure supplement 2) show that light exposure significantly reduces lateral myosin intensity compared to the dark control, while apical myosin decreases similarly in both groups. This confirms that the optogenetic manipulation selectively attenuates lateral contractility without affecting apical changes. We have added this data to the Results section.

> *(4) It would be helpful to address how heterogeneity in MRLC mutant overexpression might impact the interpretation of the outcome.*

We acknowledge that mosaic expression is common in *Ciona* electroporation. For all quantitative analyses, we only selected embryos in which the center cell and more than half of the surrounding cells in the primordium showed clear expression of the plasmid. This selection criterion has been added to the Materials and Methods section.

> *(5) For Figure 2, it would be helpful to include the en face view of the cells at different apical-basal depths to better demonstrate the changes in the subcellular localization of myosin at different stages.*

We have added top-view images in Figure 2A at both the apical and a deeper (lateral) plane. These images clearly show the ring-like localization of active myosin at the apical cell-cell junctions during the initial stage. Together with the cross-sectional views, they adequately demonstrate the subcellular localization changes.

> *(6) The Methods section should include more detailed descriptions of image quantification procedures. For example, for Figure 2B, how were the apical and lateral signals defined, and how were background intensities determined? In addition, the methods used for statistical tests should be clearly stated.*

We agree that detailed quantification procedures are essential. We have therefore expanded the Materials and Methods with a new subsection “Quantification and statistical analysis”. This subsection includes precise definitions of apical, lateral, and basal domains (segmented line, width 1 μm), background subtraction (region outside the tissue), normalization (basal intensity set to 1), and descriptions of how cell height, invagination depth, and lateral distance were measured (referencing Figure 1B). Statistical tests (two-tailed Student’s t-test) and significance levels are clearly stated.

> *(7) The discrepancies between the model and experimental data, as described above, should be acknowledged. Commentary on how the model's assumptions and setup might contribute to these differences would be helpful.*

We thank the reviewer for this suggestion. As detailed in our response to Reviewer #2 (Public Review) - Comment (6), we have included the discrepancies between the model and experimental results in the Modeling and Discussion sections. We have added comments explaining how our key modeling assumptions might contribute to these differences. Specifically, while we have updated the model to a curved geometry, the omission of continuous global tissue growth and expansion could affect the final invagination depth and

shape. Meanwhile, the neglect of mechanical interactions between the surface epithelium and the internal bulk cells prevents the model from fully capturing the constraints that refine the local furrow configuration *in vivo*. By clarifying these limitations, we now provide a more balanced view of the model's scope and its role in identifying the primary mechanical drivers of invagination.

> ***Reviewer #3 (Recommendations for the authors):***
>
> *General comments:*
>
> *(1) Methods: More information is needed to describe how imaging and quantification were performed. A couple of examples:*
>
> *(a) In Figure 1, how were the apical and basal surface area of the center cell quantified?*
>
> *(b) In Figure 1, Supplement 1, how was fluorescence intensity measured? Was there a constant area or volume that was quantified between samples? This is important because a decreasing apical surface can cause the signal to appear "concentrated" and increased.*

We thank the reviewer for this important suggestion. We have added a dedicated subsection “Quantification and statistical analysis” in the Materials and Methods. This subsection includes precise definitions of apical, lateral, and basal domains (segmented line, width 1 μm), background subtraction (region outside the tissue), normalization (basal intensity set to 1), and descriptions of how cell height, invagination depth, and lateral distance were measured (referencing Figure 1B). Statistical tests (two-tailed Student’s t-test) and significance levels are also stated.

> *(2) The manuscript could use some editing and proofreading for grammar.*

The manuscript has been carefully edited for grammar and clarity. We thank the reviewer for the suggestion.

> *Specific points:*
>
> *(1) Figure 1A: Could the authors please annotate the location of the center cell throughout the time course? This would make it easier for the reader to understand what is being quantified.*

We have added arrows to indicate the center cell at each time point in Figure 1A. This makes it easier for readers to follow the quantification.

> *(2) Figure 1 Supplement 1A, Line 143, "...before 15 hpf, F-actin concentration decreased at the lateral domains..."*
>
> *It is not clear that the graph shows a decrease in the lateral domains when taking the error bars into account. It is possible that the F-actin concentration is stable in the lateral domains before 15 hpf. Are there some statistical analyses that can be performed?*

We re-analyzed the F-actin data and agree that the change before 15 hpf is not statistically convincing given the error bars. However, we have added new quantitative analysis of active myosin (p-MLC) at 14–15 hpf (Figure 2B), which shows a clear and significant shift from lateral to apical enrichment during this early phase. This myosin dynamic strongly supports our hypothesis of bidirectional redistribution. The corresponding text has been updated in the Results section.

> *(3) Figure 1 Supplement 1A, Line 147-148, "...after 16 hpf, during which apical F-actin levels showed a gradual decline." Based on the graph, it does not appear that apical F-*

> *actin levels show a gradual decline after 16 hpf; rather, they may be steady or slightly increase.*

We agree with the reviewer. Our original statement was inaccurate. What we intended to emphasize was that at 16 hpf, the F-actin level at the lateral domain exceeded that at the apical domain. The detailed changes of F-actin after 16 hpf were not a focus of our discussion. We have revised the text accordingly to avoid any misinterpretation. The correction has been made in the Results section.

> *(4) Figure 2C Hypothesis and line 169-170, "Initially, actomyosin translocated from the lateral regions to the apical domains..."*
>
> *Related to the comment above, it is not clear that one can state that the actomyosin "translocated". The quantification does not necessarily demonstrate a loss of actin at the lateral domain in the initial stage, and even if there was a loss of lateral actomyosin, one would require experiments (perhaps photoconversion experiments) to demonstrate that machinery from the lateral region was transferred to the apical surface, rather than a process of new assembly at the apical surface.*

We fully agree with the reviewer. We have replaced the term “translocation” with “redistribution” throughout the manuscript, including the title, to avoid implying physical movement of the same actomyosin structures. The text in the Results and Discussion has been revised accordingly.

> *(5) A similar comment is relevant to the subsequent statement in line 175, "actomyosin translocated from the apical domains to the lateral regions." Without direct experiments to demonstrate movement of the actomyosin machinery, it is possible that there is de novo assembly of actomyosin in the lateral region rather than translocation.*
>
> *This wording ("translocation") becomes important primarily because it is in the title and appears to be one of the authors' major conclusions.*

We fully agree with the reviewer that the wording is critical given our main conclusion. We have therefore systematically replaced “translocation” with “redistribution” across the manuscript (title, results, and discussion).

> *(6) Figure 4, Lines 215-216, "These results confirm that the redistribution of myosin contractility from the apical to lateral regions is essential for the development of invagination."*
>
> *This experiment did not specifically test the redistribution of myosin; rather, the authors demonstrated that myosin contractility globally is necessary for invagination. In these experiments, is it known where the myosin is?*

We have performed additional immunostaining experiments (new Figure 4—figure supplement 2) to directly examine myosin distribution after optogenetic inhibition. The results show that light exposure specifically reduces lateral myosin intensity compared to the dark control, while apical myosin decreases similarly in both groups. This demonstrates that the optogenetic manipulation selectively attenuates lateral contractility. We have revised the conclusion to state that the acquisition of lateral contractility is essential for invagination progression. The new data and revised text are in the Results section.

> *(7) Figure 4B, minor point: It would be helpful if the authors included a timestamp for the bottom row images (Dark 1 h).*

Thank you for pointing out this typo. Timestamps have been added to the bottom row images (Dark 1 h) in Figure 4B.

> *(8) Figure 5E, F, minor point: It seems that the label on the red curve has a typo; it should be T18ES19E (rather than T18AS19E).*

Thank you for pointing out this typo. We have corrected it in the revised manuscript (now Figure 6A, B).

> *(9) Figure 5F and corresponding text: Can the authors please clarify what is meant by "Coupled mode" as marked in the schematic? Is this meant to refer to simultaneous apical constriction and lateral contraction? Or sequential?*

We thank the reviewer for this question. By "coupled mode," we refer to the mechanical synergy between apical and lateral contractions in driving the final invagination. As observed in our experimental data and recapitulated in the model, these two processes occur sequentially rather than simultaneously. We have revised the corresponding text to explicitly clarify this sequential process.

> *(10) Figure 6A, B, Lines 274-275: "...the invagination depth increased significantly under higher alphaa (Figure 6A), while the central height remained relatively independent of alphaa (Figure 6B)." This caused me some confusion until I realized that "Figure 6B" might be a typo and should be Figure 6C.*

We sincerely apologize for this confusion. In the revised manuscript, this specific section and the corresponding figures have been updated.

> *(11) Line 287, typo: I believe that "Figure 5B" should be Figure 6B.*

We sincerely apologize for this confusion. In the revised manuscript, this specific section and the corresponding figures have been updated.

> *(12) Figure 6A, B, comparing invagination depth with varying apical or lateral actomyosin intensity: The authors state that "invagination depth increased significantly under higher alphaa", but describe "mild invagination depth variation" with varied lateral actomyosin intensity. The graphs seem to suggest that there is increased invagination depth when either apical or lateral actomyosin intensity is increased, and that the increase is to a similar extent. Can the authors comment on what they think the differences are, if the apical effect is "significant" but the lateral effect is "mild"?*

We thank the reviewer for this meticulous observation. We agree and feel sorry that our original description was not sufficiently precise. In the revised manuscript, we have re-analyzed the distinct contributions of apical and lateral tensions using the updated curved vertex model, which provides a more accurate mechanical decoupling. We have accordingly replaced the previous wording with a more rigorous description of the simulations and streamlined the corresponding figures to ensure the conclusions are clearly supported.

> *(13) Figure 6H, Lines 307-309, "...stronger regional translocation and redistribution contribute to the rapid reduction in height of invaginating cells..."*
>
> *It appears from the graph that this is really only apparent at high alpha (total actomyosin); at empirically determined levels (alpha = 1), the effect of varying ratio is less dramatic. Can the authors comment on how significant they consider this effect?*

We thank the reviewer for this insightful comment. We agree that the theoretical predictions regarding translocation strength in the original model lacked sufficient experimental validation. To maintain the scientific rigor of our study, we have removed the sections concerning the translocation ratio and the corresponding Figure 6H from the revised manuscript. Instead, we now refocus our analysis on the core mechanical drivers of invagination that are directly supported by our observations. We also have added discussions

acknowledging other factors not fully captured in the current model (e.g., tissue growth), which we aim to investigate in future work.

https://doi.org/10.7554/eLife.108588.2.sa0